INL/RPT-23-72192

Gas-Cooled High-Temperature Pebble-Bed Reactor Reference Plant Model

April 2023

Mustafa Jaradat[1], Sebastian Schunert[1], and Javier Ortensi[1]

[1]*Reactor Physics Methods and Analysis*

Idaho National Laboratory

INL is a U.S. Department of Energy National Laboratory
operated by Batelle Energy Alliance, LLC

DISCLAIMER

This information was prepared as an account of work sponsored by an agency of the U.S. Government. Neither the U.S. Government nor any agency thereof, nor any of their employees, makes any warranty, expressed or implied, or assumes any legal liability or responsibility for the accuracy, completeness, or usefulness, of any information, apparatus, product, or process disclosed, or represents that its use would not infringe privately owned rights. References herein to any specific commercial product, process, or service by trade name, trade mark, manufacturer, or otherwise, does not necessarily constitute or imply its endorsement, recommendation, or favoring by the U.S. Government or any agency thereof. The views and opinions of authors expressed herein do not necessarily state or reflect those of the U.S. Nuclear Regulatory Commission.

INL/RPT-23-72192

Gas-Cooled High-Temperature Pebble-Bed Reactor Reference Plant Model

Mustafa Jaradat[1], **Sebastian Schunert**[1], **and Javier Ortensi**[1]

[1]**Reactor Physics Methods and Analysis**

April 2023

Idaho National Laboratory
Nuclear Science and Technology
Idaho Falls, Idaho 83415

http://www.inl.gov

Prepared for the
Office of Nuclear Regulatory Research
U. S. Nuclear Regulatory Commission
Washington, D. C. 20555
Task Order No.: 31310019F0015

Page intentionally left blank

SUMMARY

This report details a fully coupled neutronics thermal hydraulics reference plant model for a gas-cooled high-temperature pebble-bed reactor. The multiphysics model is developed on the Nuclear Regulatory Commission's Comprehensive Reactor Analysis Bundle available on the Idaho National Laboratory high-performance computer, which natively and seamlessly couples Griffin, Pronghorn, and the BISON Multiphysics Object-Oriented Simulation Environment–based applications. Griffin provides the reactor physics capabilities, including depletion to the equilibrium core, k-eigenvalue, adjoint, and transient solutions. Pronghorn solves the porous medium equations for the fluid regions and conduction in the solid regions. BISON solves thermal conduction problems for the average and tristructural isotropic pebbles in the pebble-bed core thus providing the fuel and moderator spatial fields for each pebble burnup group. The neutronics feedback relies primarily on fuel and moderator temperatures. This report presents our results for the coupled steady state equilibrium core and a protected loss of flow event. Although this model is prototypical regarding capabilities in the Comprehensive Reactor Analysis Bundle, its results are consistent with published work by the Institute of Nuclear and New Energy Technology in China and other research entities.

ACKNOWLEDGEMENTS

This research made use of the resources provided by the Nuclear Energy Advanced Modeling and Simulation program managed by the Department of Energy Office of Nuclear Energy.

This research made use of the resources of the High Performance Computing Center at Idaho National Laboratory, which is supported by the Office of Nuclear Energy of the U.S. Department of Energy and the Nuclear Science User Facilities under Contract No. DE-AC07-05ID14517.

Description of the various author roles:

- Mustafa Jaradat—neutronics model development and multiphysics analysis
- Javier Ortensi—conceptual development, cross sections, neutronics model development, multiphysics analysis
- Sebastian Schunert—conceptual development, code development (Nuclear Energy Advanced Modeling and Simulation), thermal fluids model development

This work would not have been possible without the contributions from the Idaho National Laboratory Griffin development team: Yaqi Wang, Sebastian Schunert, Zach Prince, Vincent Labouré, Josh Hanophy, and Olin Calvin.

We are grateful to all Multiphysics Object-Oriented Simulation Environment developers that supported this work, including Alexander Lindsay, Logan Harbour, Guillaume Giudicelli, and Derek Gaston.

Page intentionally left blank

CONTENTS

FIGURES

TABLES

ACRONYMS

CCCP	current-coupled collision probability
DLOFC	depressurized loss of forced cooling
HTR-PM	high-temperature gas-cooled reactor pebble-bed module
INL	Idaho National Laboratory
KLAK	Kleine Absorber Kugel Systeme
KTA	Kerntechnischer Ausschuss
MOL	middle of life
MOOSE	Multiphysics Object-Oriented Simulation Environment
NEAMS	Nuclear Energy Advanced Modeling and Simulation
NRC	Nuclear Regulatory Commission
PBR	pebble-bed reactor
SOW	statement of work

Page intentionally left blank

1. INTRODUCTION

This report details the progress and activities of Idaho National Laboratory (INL) in regard to the Nuclear Regulatory Commission (NRC) project "Development and Modeling Support for Advanced Non-Light Water Reactors."

Table 1 provides a summary of completed tasks documented in this report. The table matches the deliverable number, statement of work (SOW) task, and (short) description of the deliverable. This report is organized as in the following. Section 2 provides a brief design description of the reference HTR-PM. Section 3 discusses the cross section generation procedure with analysis methodology used in this work. In Section 4, the developed models of the HTR-PM are described and Section 5 presents the equilibrium core results and the depressurized loss of forced cooling DLOFC transient. Finally, the summary and future work are provided in Section 6 and Section 7.

Table 1: List of deliverables and tasks.

Deliverable Number	SOW Task	Description
15	15b	Support for improvements to the reference plant model (Task 6*) to account for actual design information
15	15c	Improvements in bypass flow modeling when actual design details become available
15	15d	Support for developing microscopic cross sections and the potential use of equivalence theory for gas-cooled pebble-bed cores

* Task 6 entailed modifying the "reference plant" input model for the high-temperature gas-cooled reactor pebble-bed module (HTR-PM) to perform a coupled thermofluid and neutronics transient calculation of a depressurized loss of forced cooling (DLOFC) event. The thermofluid analysis shall be conducted using the full momentum equation formulation in Pronghorn with all significant flow paths modeled.

2. REACTOR DESIGN DESCRIPTION

The HTR-PM design is based on the combined experience from the German pebble-bed reactor program from the 1960s through the 1990s and the HTR-10 experience in China [7] during the 2000s. Currently, two HTR-PM reactors are in operation at the Shidao Bay nuclear power plant in China. We selected the HTR-PM reactor for this study because of 1) the availability of open literature data, 2) it is the only pebble-bed reactor currently in operation, and 3) its design is contemporaneous with past concepts.

The HTR-PM reactor layout can be found in Reference [3]. The main characteristics include a cylindrical pebble-bed region surrounded by radial, top cavity, lower, and upper reflectors. The radial reflector includes various orifices for the control rod channels, Kleine Absorber Kugel Systeme (KLAK) channels (shutdown system), and fluid riser channels. The HTR-PM design specifications are listed in Table 2.

Table 2: HTR-PM core specifications [2, 3].

Parameter	Value
Core power [MWth]	250.00
Core inlet temperature [K]	523.15
Core outlet temperature [K]	1023.15
Core outlet pressure [MPa]	7.0
Pebble-bed radius [m]	1.50
Pebble-bed height [m]	11.00
Reflector outer radius [m]	2.50
Control rods channels	24
Reactivity Shutdown Channels	4
Barrel outer radius [m]	2.69
Bypass outer radius [m]	1.69
Vessel outer radius [m]	3.00
Number of pebbles	419,384 (420,000)
Pebble types	1 pebble type
Pebble packing fraction (average)	0.61
Average number of passes	15
Average pebble residence time [days]	70.5

The pebble and TRISO design specifications used in the equilibrium core are included in Tables 3 and 4, respectively. These specifications are based on the uranium oxide fuel tested in the HTR-10 prototype[5]. There are some discrepancies in the buffer layer thickness from the refer-

ences, 90 μm in [6] versus 95 μm in [5]. We opted for the 90 μm design.

Table 3: HTR-PM pebble specifications [2, 4].

Parameter	Value
Fueled region radius [cm]	2.5
Shell layer thickness [cm]	0.5
Pebble diameter [cm]	6.0
Heavy metal loading per pebble [g]	6.95
Number of particles per pebble	11,668
Particle packing [%]	7.034
Discharge burnup [MWd/kg, J/m^3]	90, 4.82×10^{14}
Fuel layer matrix density [kg/m^3]	1,730
Shell layer graphite density [kg/m^3]	1,730

Table 4: HTR-PM TRISO particle specifications [5, 6].

Parameter	Value
Fuel kernel radius [cm]	0.025
Buffer outer radius [cm]	0.034
IPyC outer radius [cm]	0.038
SiC outer radius [cm]	0.0415
OPyC outer radius [cm]	0.0455
Particle diameter [cm]	0.091
Fuel type	UO_2
Fuel enrichment	8.6%
Fuel kernel density [kg/m^3]	10,400
Buffer graphite density [kg/m^3]	1,100
IPyC, OPyC graphite density [kg/m^3]	1,900
SiC density [kg/m^3]	3,180

3. ANALYSIS METHODOLOGY

In this work, a multiphysics reference plant model of the HTR-PM was developed based on the Multiphysics Object-Oriented Simulation Environment (MOOSE) [8–10]. The multiphysics model consists of four models coupled using the MultiApp system: (1) Griffin neutronics model, (2) Griffin depletion model, (3) Pronghorn thermal-hydraulics model, and (4) pebble and TRISO temperature model. Section 3.1 briefly introduces the reactor physics methods used in this work, while the Pronghorn methodology is described in Section 3.2.

3.1 Reactor Physics Methods

Griffin is a reactor multiphysics application built on MOOSE and is based on the technology developed for Rattlesnake [11], Mammoth [12], and PROTEUS [13]. Griffin provides neutron transport, depletion, core performance, decay heat, and cross-section calculation capabilities for non-light-water advanced reactor technologies. In this work, we used Griffin's diffusion approximation to solve the linearized Boltzmann transport equation with the multigroup approximation in the energy domain. In order to perform neutronics and depletion calculations with Griffin, multigroup cross sections need to be provided as a function of reactor state parameters, such as temperature and burnup.

3.1.1 Multigroup Cross-Section Generation Procedure

The cross-section preparation capability for PBRs in Griffin is not currently available but should be ready for testing at the end of Fiscal Year 2023. In lieu of Griffin cross sections, we relied on DRAGON [14, 15] to prepare microscopic cross sections for this work. DRAGON is a lattice physics code developed at École Polytechnique de Montréal as part of the Version 5 package [16]. DRAGON includes a number of transport solvers and self-shielding models that have been in use at INL.

The DRAGON data libraries used in this work are based on the ENDF/B-VIII.r0 evaluation. For the neutron self-shielding method, the SHEM 281 group library was used with the subgroup projection method [17]. The double heterogeneity treatment is based on the Hébert method. A current-coupled collision probability (CCCP) flux solution is used for spatial homogenization and

energy condensation of microscopic cross sections. The intracore neutron leakage affects the local spectrum significantly, and it will have an impact on the cross-section homogenization. Nevertheless, this approach with the generated cross sections serves as an initial set to perform preliminary calculations until more sophisticated methods are available in Griffin. The nominal depletion conditions are provided in Table 5.

Table 5: Main DRAGON depletion parameters. The average fuel and moderator temperatures are taken from preliminary thermal fluids solutions with Pronghorn. The neutron flux was obtained from a DRAGON-5 depletion calculation at constant power at the middle of life (MOL)

Parameter	Value
Tfuel	898.0 K
Tmod	803.0 K
Neutron flux	$1.521 \times 10^{14}\,\mathrm{n/cm^2/s}$

We used two geometric representations in DRAGON, depicted in Figure 1, to compute the microscopic cross sections: (a) pebble and (b) pebble ensemble.

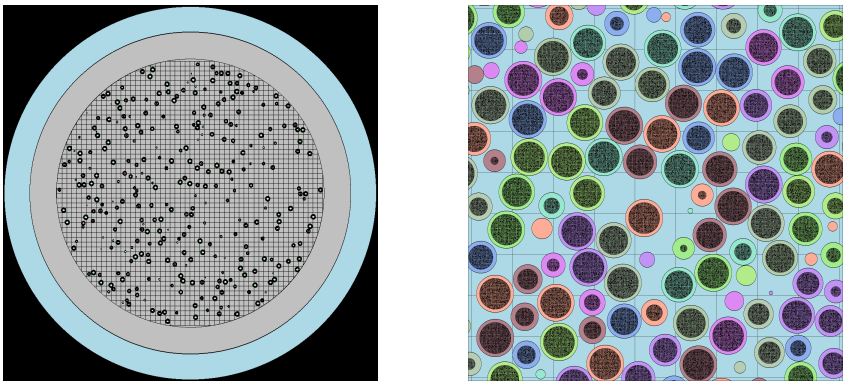

(a) Pebble (b) Pebble ensemble

Figure 1: Geometric representation of the single pebble and pebble ensemble. Figures generated with Serpent.

The following one-dimensional (1D) spherical calculations are performed:

1. Single pebble depletion at a constant power to obtain a flux level at middle of life (MOL)
2. Single pebble depletion at a constant flux
3. Single pebble depletion at a constant flux in a pebble ensemble with middle of life (MOL) ($\sim$528 days) compositions from Step 1

4. Pebble branch cases with isotope concentrations from Step 2 in a MOL pebble ensemble.

The microscopic cross sections are condensed from 281 to nine energy groups and homogenized over the pebble. The nine energy groups structure is provided in Table 6. The isotope transport cross sections are based on a "flux-limited" approximation [18] or in-scatter approximation with scalar flux as a weighting function [19]:

$$\sigma_{tr}^{g} = \sigma_{t}^{g} - \sum_{g'=1}^{G} \sigma_{s_1}^{g'->g} \frac{\phi_0^{g'}}{\phi_0^{g}}. \tag{1}$$

The top void transport cross sections were calculated in Serpent with the cumulative migration method [18]. The inverse velocities are derived from the broad group structure energies. The delayed neutron fraction is based on a (β_0) formulation in a matrix form to represent the dependence on the broad energy and delayed neutron precursor groups.

Table 6: Neutron energy group boundaries for the nine group structure. Based on the General Atomics 9-group structure [20] matched to nearest DRAGON-5 energy boundaries.

Group	Upper Energy [eV]	Lower Energy [eV]
1	1.96403000E+07	1.95007703E+05
2	1.95007703E+05	9.07500671E+02
3	9.07500671E+02	1.75647602E+01
4	1.75647602E+01	3.88216996E+00
5	3.88216996E+00	2.33006096E+00
6	2.33006096E+00	1.29303801E+00
7	1.29303801E+00	8.20037127E-01
8	8.20037127E-01	1.37999400E-01
9	1.37999400E-01	1.10002700E-04

The reactor feedback mechanism in the HTR-PM is attributed to changes in the following temperatures:

- Fuel: Average temperature in the UO_2 kernel for each pebble type and each burnup group
- Moderator: Average pebble temperature for each pebble type and each burnup group
- Reflector: Local temperature of the graphite reflector.

The tabulation values for the cross sections are shown in Table 7 and are intended for supporting transient analyses.

Table 7: Microscopic cross-section tabulation parameters of the HTR-PM.

Parameter	Value
Number of isotopes	294
Burnup tabulation [days]	0.0, 528, 1254
Burnup tabulation [MWd/kg]	0.0, 52.2, 100.8
Burnup tabulation [J/m^3]	0.00, $2.789\,17 \times 10^{14}$, $5.389\,49 \times 10^{14}$
Fuel temperature tabulation [K]	500.0, 700.0, 900.0, 1100.0, 1300.0, 1600.0, 2000.0
Moderator temperature tabulation [K]	300.0, 500.0, 700.0, 900.0, 1100.0, 1300.0, 1600.0, 2000.0

3.1.2 Equilibrium Core Calculations

The equilibrium core is attained via the streamline depletion method available in Griffin [21]. In this depletion approach, a 2D and 3D core flux solution is mapped to 1D axial streamlines. A set of 1D steady-state advection-transmutation equations for all isotopes are solved in each streamline. Griffin assumes that the pebble loading and unloading rates are identical.

The fraction of volume occupied by pebbles (i.e., packing fraction) on streamline k at position s is denoted by $n_k(s)$.

$$n_k(s) = \text{Packing fraction} = \frac{\text{Volume occupied by pebbles}}{\text{Total volume}}. \tag{2}$$

The definition on the right-hand side of Equation 2 is to be understood as follows: at location s along streamline k, a representative volume centered at s is selected that contains a sufficient number of pebbles. The total extent of this representative volume is the denominator of Equation 2, while the portion occupied by the pebbles is the numerator. Both the numerator and denominator on the right-hand side of Equation 2 depend on s and index k, but we omitted these details for the sake of brevity. We treated $n_k(s)$ as a continuous function, implying that $n_k(s)$ can be meaningfully evaluated at a given point, even though the definition of $n_k(s)$ requires a representative volume of finite size.

The fraction of pebble volumes is related to the porosity by $n_k(s) = 1 - \epsilon_k(s)$. The steady-state balance equation for $n_k(s)$ is:

$$u_k(s)A_k(s)n_k(s) = u_k(s)A_k(s)(1 - \epsilon_k(s)) = \text{constant along streamline} = \dot{n}_k. \tag{3}$$

where $u_k(s)$ is the speed of pebbles tangential to streamline k at location s, $A_k(s)$ is the cross-sectional area of streamline k at distance s from the streamline inlet measured perpendicular to the tangent along the streamline, and $\dot{n}_k$ is the volumetric flow rate of pebbles on streamline k (i.e., the volume of pebbles that leave streamline k per unit time). These equations allow for computing the speed of pebbles $u_k(s)$ for any location along the streamline via the streamline geometry, local porosity, and rate at which pebbles are introduced into the streamline at the pebble inlet.

In PBRs, different types of pebbles (different fuel compositions, graphite pebbles, burnable absorber pebbles) can be present at the same time. We denote the volume fraction occupied by a pebble of type c, as identified by its initial composition on streamline k, by $n_{c,k}$. The volume fraction $n_{c,k}(s,\tau)$ depends on the distance (s) measured along the streamline from the core inlet and on burnup (τ):

$$n_{c,k}(s,\tau)d\tau = \frac{\left[\begin{array}{l}\text{Volume occupied by a pebble of type } c \text{ identified by initial composition} \\ \text{on streamline } k \text{ with burnup between } \tau \text{ and } \tau + d\tau\end{array}\right]}{\text{Total volume}}. \quad (4)$$

The relationship between $n_{c,k}(s,\tau)$ and $n_k(s)$ is:

$$n_k(s) = \sum_{c=1}^{C} \int_0^{\infty} n_{c,k}(s,\tau)d\tau. \quad (5)$$

The balance equation for $n_{c,k}(s,\tau)$ along the streamline is given by:

$$\frac{\partial\left(u_k(s)A_k(s)n_{c,k}(s,\tau)\right)}{\partial s} + A_k(s)\frac{\partial\left(\overline{p}_c(\vec{r}_k(s),\tau)n_{c,k}(s,\tau)\right)}{\partial \tau} = 0, \quad (6)$$

where $\overline{p}_c(\vec{r}_k(s),\tau)$ is the power density that a pebble of type c with a burnup between τ and $\tau + d\tau$ experiences. The volume fraction occupied by pebbles of type c with burnups falling into group b is given by:

$$n_{c,k,b}(s) = \int_{\tau_b}^{\tau_{b+1}} n_{c,k}(s,\tau)d\tau. \quad (7)$$

Integrating Equation 6 over τ within $[\tau_b, \tau_{b+1}]$ gives:

$$\frac{\partial\left(u_k A_k n_{c,k,b}(s)\right)}{\partial s} + A_k\left[\overline{p}_c(\tau_{b+1})n_{c,k}(\tau_{b+1}) - \overline{p}_c(\tau_b)n_{c,k}(\tau_b)\right] = 0, \quad (8)$$

where obvious arguments are omitted for convenience of notation. We approximate $\overline{p}_c(\tau_b)n_{c,k}(s,\tau_b)$ using upwinding in the direction of increasing burnup:

$$\overline{p}_c(\tau_b)n_{c,k}(\tau_b) \approx \begin{cases} 0 & \text{if } b = 1 \\ 0 & \text{if } b = B+1 \\ \frac{\overline{p}_{c,b-1}n_{c,k,b-1}}{\Delta\tau_{b-1}} & \text{else} \end{cases}, \tag{9}$$

where $\Delta\tau_b = \tau_{b+1} - \tau_b$ and the average power is defined by:

$$\overline{p}_{c,b}(\vec{r}_k(s)) = \frac{1}{\Delta\tau_b}\int_{\tau_b}^{\tau_{b+1}} \overline{p}_c(\vec{r}_k(s),\tau)d\tau. \tag{10}$$

This result leads to the semidiscrete form of Equation 8:

$$\frac{\partial\left(u_k A_k n_{c,k,b}\right)}{\partial s} + A_k\left[\frac{\overline{p}_{c,b}n_{c,k,b}}{\Delta\tau_b} - \frac{\overline{p}_{c,b-1}n_{c,k,b-1}}{\Delta\tau_{b-1}}\right] = 0. \tag{11}$$

This equation couples the population of pebbles in burnup group b at location s to the neighboring burnup group $b-1$ and neighboring locations in space. When discretizing the derivative with respect to τ, we used a constant approximation of power over each burnup group (i.e., $\overline{p}_c(\vec{r}_k(s),\tau) \approx \overline{p}_{c,b}(\vec{r}_k(s))$). We denote the concentration of isotope q contained in a pebble of type c traversing the core on streamline k by $N_{q,c,k}$. The concentration $N_{q,c,k}(s,\tau)$ depends on the distance (s) measured along the streamline from the core inlet and on burnup (τ):

$$N_{q,c,k}(s,\tau)d\tau = \frac{\left[\begin{array}{l}\text{Number of atoms of isotope } q \text{ in pebbles with initial composition } c \\ \text{on streamline } k \text{ with burnup between } \tau \text{ and } \tau + d\tau\end{array}\right]}{\text{Total volume}}. \tag{12}$$

It is convenient to collect the different isotopes in the vector $\vec{N}_{c,k}$ that contains the concentration $N_{q,c,k}$ as its q^{th} entry. The balance equation for $\vec{N}_{c,k}(s,\tau)$ along the streamline is given by:

$$\frac{1}{A_k(s)}\frac{\partial\left(u_k A_k \vec{N}_{c,k}\right)}{\partial s} + \frac{\partial\left(\overline{p}_c\vec{N}_{c,k}\right)}{\partial\tau} = \mathbf{\Lambda}(\phi)\vec{N}_{c,k}(s,\tau), \tag{13}$$

where $\mathbf{\Lambda}(\phi)$ is the transmutation and decay matrix that depends on the neutron flux ϕ. The entries

in the transmutation and decay matrix are:

$$\begin{aligned}\mathbf{\Lambda}_{q,q} &= -\lambda_q - \sigma_{\mathrm{tr},q}\overline{\phi}, \\ \mathbf{\Lambda}_{q,m} &= \lambda_m \gamma^d_{m\to q} + \sigma_{\mathrm{tr},m}\gamma^a_{m\to q}\overline{\phi},\end{aligned} \tag{14}$$

where λ_q is the decay constant of isotope q, $\sigma_{\mathrm{tr},q}$ is the collapsed microscopic transmutation cross section of isotope q (i.e., a cross section that collects all reactions that "destroy" isotope q) evaluated on the neutronics domain, $\overline{\phi}$ is the collapsed one-group scalar flux averaged from the neutronics domain to the streamline, $\gamma^d_{m\to q}$ is the fraction of isotope m decays leading to the creation of isotope q (i.e., the branching ratio), and $\gamma^a_{m\to q}$ is the fraction of neutron transmutation reactions for isotope m leading to the creation of isotope q. Analogous to $n_{c,k,b}$, we define $\vec{N}_{c,k,b}$ as:

$$\vec{N}_{c,k,b} = \int_{\tau_b}^{\tau_{b+1}} \vec{N}_{c,k}(s,\tau)d\tau. \tag{15}$$

Integrating Equation 13 and using the same discretization as for Equation 11 leads to:

$$\frac{1}{A_k(s)}\frac{\partial\left(u_k A_k \vec{N}_{c,k,b}\right)}{\partial s} + \left[\frac{\overline{p}_{c,b}\vec{N}_{c,k,b}}{\Delta\tau_b} - \frac{\overline{p}_{c,b-1}\vec{N}_{c,k,b-1}}{\Delta\tau_{b-1}}\right] = \mathbf{\Lambda}\vec{N}_{c,k,b}. \tag{16}$$

With $\vec{N}_{c,k,b}$ defined, we define the average power, $\overline{p}_{c,b}$, by:

$$\overline{p}_{c,b}(\vec{r}_k(s)) = \sum_{q=1}^{Q}\sum_{g=1}^{G}\frac{N_{q,c,k,b}}{n_{c,k,b}}\kappa\sigma_{f,q,g}(\overline{T})\overline{\phi}_g, \tag{17}$$

where $\overline{\phi}_g$ is the group scalar flux averaged from the neutronics domain to the streamline, $\overline{T}$ is the temperature transferred to the streamline, and the number density $N_{q,c,k,b}$ is the number of type q atoms divided by the total volume. However, to compute the average power density in type c pebbles within burnup groups b, we need to use the isotope number density computed with the volume of pebble type c and burnup group b. This quantity is given by $N_{q,c,k,b}/n_{c,k,b}$. The average pebble power density, $\overline{p}_{c,b}$, is related to the average reactor power density by:

$$\overline{p}(\vec{r}) = \sum_{c,b} n_{c,k,b}\overline{p}_{c,b}(\vec{r}_k(s)), \tag{18}$$

which is a weighted average over the different pebble types. Note that $\overline{p}(\vec{r})$ is the power density with respect to the entire volume (i.e., total power divided by reactor volume and **not** pebble volume).

3.1.3 Decay Heat Calculation

A decay heat model was added for the equilibrium core model to properly perform the loss of forced cooling transients. The decay heat source is mainly important for transient analyses when the fission power is reduced to zero due to negative reactivity insertion. In steady state, the decay heat is assumed to be included in the energy released per fission, and, thus, assumed to have the same distribution as the prompt fission power. In this decay heat model, the fission products are grouped into a few decay heat precursor groups (K_D), and each group has its unique decay heat fraction (f_k) and constant (λ_k). Then, the following time-dependent decay heat precursor equation is solved for each group analytically:

$$\frac{\partial h_k(\vec{r},t)}{\partial t} + \lambda_k h_k(\vec{r},t) = f_k \sum_{g=1}^{G} \kappa_f \Sigma_{fg}(\vec{r},t)\phi_g(\vec{r},t), \qquad k = 1, 2, ..., K_D, \tag{19}$$

where h_k denotes the decay heat precursor group k and κ_f is the recoverable energy per fission. Equation 19 can be solved analytically over a time-step size of Δt assuming the neutron flux solution and cross sections remain constant during that time step, resulting in:

$$h_k(\vec{r},t) = h_k(\vec{r},t-\Delta t)e^{-\lambda_k \Delta t} + \frac{(1-e^{-\lambda_k \Delta t})}{\lambda_k} f_k \sum_{g=1}^{G} \kappa_f \Sigma f g \phi_g. \tag{20}$$

Then the total heat source P_{total} is defined as the summation of prompt fission heat P_{prompt} and decay heat source P_{decay}:

$$P_{total}(\vec{r},t) = P_{prompt}(\vec{r},t) + P_{decay}(\vec{r},t), \tag{21}$$

$$P_{prompt}(\vec{r},t) = (1 - \sum_{k=1}^{K_D} f_k) \sum_{g=1}^{G} \kappa_f \Sigma_{fg} \phi_g, \tag{22}$$

$$P_{decay}(\vec{r},t) = \lambda_k h_k(\vec{r},t). \tag{23}$$

In order to evaluate Equation 20, the decay heat fraction and constants must be determined for each group. The delayed heat groups can be obtained by fitting the delayed energy released

by fission products as a function of the emission time. For light-water reactors, the 2014 ANS decay heat standard includes the time-dependent decay energy as an exponential fit from the direct fission of four important fissionable isotopes ^{235}U, ^{238}U, ^{239}Pu, and ^{241}Pu. In this standard, the decay heat power is represented as a summation of 23 exponential terms [22]. In the current work, a similar procedure was adopted to represent the decay heat with exponential fitting as a summation of K exponential terms as:

$$P_{decay}(t) = P_{decay,0} \sum_{k=1}^{K_D} f_k e^{-\lambda_k t}, \tag{24}$$

where $P_{decay,0}$ is the decay heat generated during a steady-state operation before reactor shutdown. Then, the decay heat fraction and decay constant for each group can be determined from the exponential fitting of the decay heat curve after performing depletion calculations at full power for a sufficient amount of time so that the decay heat reaches a saturation or equilibrium level. Then, shutdown conditions are imposed, and the decay heat is calculated.

In this work, the time-dependent decay heat values after reactor shutdown were taken from Reference [1], as shown in Figure 2, along with fitting curve of the decay heat. An exponential fitting with six decay heat groups were considered to obtain a fitting parameter of the exponential terms as provided in Table 8.

Table 8: Decay heat fitting parameters.

Group	Fraction [%]	Decay Constant [s^{-1}]
1	0.99013	3.65752E-01
2	1.32799	5.99835E-04
3	1.45738	5.65974E-02
4	1.36383	7.74312E-03
5	0.67246	5.39475E-05
6	0.60207	1.87351E-06
Total	6.41387	

During transient calculations, the decay heat is scaled with the steady-state relative fission power of each mesh, and time-dependent decay heat precursors equation was solved during transients for each group.

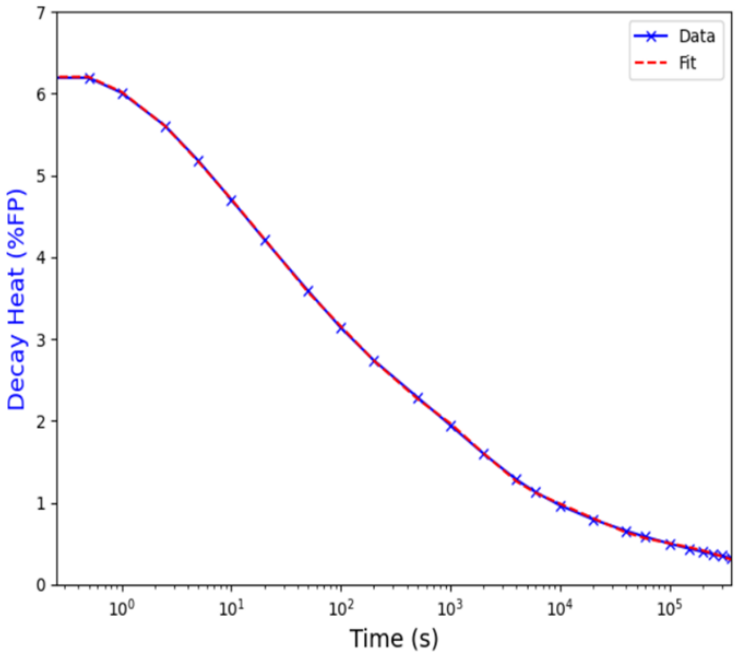

Figure 2: Evolution of decay heat with time Reference [1], and fitted values after shutdown.

3.2 Thermal Fluids Methods

Pronghorn is another MOOSE-based application that solves the solid and fluid equations with a porous medium approximation in porous zones. A weakly compressible finite volume formulation is used for discretizing the fluid mass, fluid momentum, fluid energy, and solid energy conservation equations. All equations solved are time dependent and described in detail in Reference [23]. In addition, we used the correlations available in Pronghorn [24] to compute the effective thermophysical properties of the porous media. The equations solved are a typical porous media formulation of the Navier-Stokes equations. This is a low mach formulation called "Weakly Compressible" within the code in witch the dependency of the variables from pressure is dropped in several terms. The momentum equation is altered from the traditional Navier-Stokes relationship by replacing the viscous diffusion term with a porous friction term comprised of Darcy and Forchheimer correlated friction relationships. The mass conservation equation is a standard porosity weighted equation. Equations 25, 26, and 27 show the porous media mass, momentum, and energy conservation equations, respectively, which are then solved using a finite-volume discretization scheme using Rhie-Chow interpolation.

The fluid and solid energy conservation equations are handled distinctly and are coupled

through a heat transfer coefficient. As a result, the solid temperature field must be solved to fully define the system. This solution is based on the solid energy conservation equation seen in Equation 28, which includes internal heat generation to take into account the heat produced within the fuel. The average graphite and TRISO temperatures are computed using spherically symmetric, 1D subscale heat conduction models in each pebble-bed mesh element.

$$\frac{\partial \epsilon \rho_f}{\partial t} + \nabla \cdot (\epsilon \rho_f \vec{v}) = 0, \tag{25}$$

$$\rho_f \frac{\partial \vec{v}}{\partial t} + \frac{\rho_f}{\epsilon}(\vec{v} \cdot \nabla)\vec{v} + \epsilon \nabla p - \epsilon \rho_f \vec{g} + W \rho_f \vec{v} = 0, \tag{26}$$

$$\epsilon \rho_f C_{p,f} \frac{\partial T_f}{\partial t} + \epsilon \rho_f C_{p,f} \nabla \vec{v} \cdot (T_f) - \nabla \cdot (\epsilon \kappa_f \nabla T_f) + \alpha (T_f - T_s) = \dot{q}'''_f, \tag{27}$$

$$(1 - \epsilon) \rho_s C_{p,s} \frac{\partial T_s}{\partial t} - \nabla \cdot (\kappa_s \nabla T_s) + \alpha (T_s - T_f) = \dot{q}'''_s. \tag{28}$$

where ϵ is the pebble-bed porosity, $\epsilon \vec{v}$ is the superficial velocity, $\vec{v}$ is the real or intrinsic velocity, and the subscripts f and s denote the liquid and solid phases, respectively.

3.2.1 Effective Thermal Properties

Using porous media to model a pebble bed requires several correlations to obtain effective bed properties. For the fluid momentum equations, this translate into specific corelations for the Darcy and Forchheimer coefficients to capture the large additional resistances caused by the constrained tortuous flows. Similarly, the fluid and solid thermal properties need to be properly resolved in a homogenized manner to obtain accurate temperature distributions. Within the fluid region, the only needed effective property is the effective conductivity of the fluid κ_f in the porous media in Equation 27. The effective conductivity of the fluid generally increases with Reynolds and Prandtl numbers and is handled with the linear Peclet model as:

$$\kappa_f = \epsilon k_f + C_0 Pe k_f. \tag{29}$$

Similarly, the solid region effective conductivity κ_s in Equation 28 is needed, and it is more complicated to obtain as a pebble-bed reactor will have more interaction modes from pebble to pebble than the fluid does across the pebbles. The interaction modes are radiation between pebbles, di-

rect conduction between pebbles in the contact area, and pebble conduction through fluid between pebbles. Then, the solid effective conductivity can be represented as:

$$\kappa_s = \kappa_{\text{radiation}} + \kappa_{\text{solid conduction}} + \kappa_{\text{fluid conduction}}. \tag{30}$$

For the radiation component of the solid effective conductivity, the Breitbach and Barthels model was used as:

$$\kappa_{\text{radiation}} = \left[\left(1 - \sqrt{1-\epsilon}\right) \epsilon + \frac{\sqrt{1-\epsilon}}{2/\epsilon_{r,s} - 1} \frac{B+1}{B} \frac{1}{1 + \frac{1}{(2/\epsilon_{r,s}-1)\Lambda}} \right] 4\sigma d_p \bar{T}^3. \tag{31}$$

The pebble-to-pebble conduction is handled with the Chan and Tien model, and the pebbles conduction through fluid component is handled with the Zehner, Bauer, and Schlunder (ZBS) model as:

$$\begin{aligned} \kappa_{\text{solid conduction}} &= \frac{1}{2 \cdot 0.53} \frac{N_A}{N_L} \left(\frac{d_c}{d_p}\right) d_p \lambda k_f \\ \kappa_{\text{fluid conduction}} &= (1 - \sqrt{1-\epsilon}) k_f + \sqrt{1-\epsilon} K_{SF} k_f. \end{aligned} \tag{32}$$

The heat transfer coefficient α that couples the solid energy equation, Equation 28, and the fluid energy equation, Equation 27, is determined based on the Kerntechnischer Ausschuss (KTA) model. The heat transfer coefficient then acts as a volumetric source coefficient where the local fluid energy source, and subsequently solid energy sink, is proportional to the difference between the solid and fluid temperatures locally. The heat transfer coefficient is obtained via correlations using Nusselt number formulations as:

$$Nu = 1.27 \frac{Pr^{1/3} Re^{0.36}}{\epsilon^{1.18}} + 0.033 \frac{Pr^{0.5} Re^{0.86}}{\epsilon^{1.07}}. \tag{33}$$

Equation 33 is valid for a bed height greater than four times the pebble diameter and $0.36 < \epsilon < 0.42$, $100 < Re < 10^5$, and $Pr = 0.7$. Further detail is in the Pronghorn user manual and referenced sources within Reference [24].

3.2.2 Modeling of Stagnant Gas Gaps

Modeling the heat transfer across stagnant gas gaps uses a simple effective thermal conductivity model. This model treats the gap as if it is filled with an effective material with a thermal conductivity adjusted to keep into account both conduction and radiation trough the gap. The effective thermal conductivity is given by:

$$\kappa_s = \kappa_C + \kappa_R, \tag{34}$$

where k_C is the conduction component and k_R is the radiation component. The radiation component cylindrical gaps are determined from:

$$2k_R\pi H\frac{T_1 - T_2}{\log\left(\frac{R_2}{R_1}\right)} = \frac{A_1\sigma\left(T_1^4 - T_2^4\right)}{\frac{1}{\epsilon_1} + \frac{1-\epsilon_2}{\epsilon_2}\frac{R_2}{R_1}}, \tag{35}$$

where Indices 1 and 2 are the two sides of the gap, ϵ is the emissivity, σ is the Stefan-Boltzmann constant, A_1 is the area of Surface 1, R_1 and R_2 are the radii of Surface 1 and 2, respectively, and H is the height. The ultimate expression for k_R is:

$$k_R = 4\sigma T^3\frac{R_1\log\left(\frac{R_2}{R_1}\right)}{\frac{1}{\epsilon_1} + \frac{1-\epsilon_2}{\epsilon_2}\frac{R_2}{R_1}}. \tag{36}$$

The gap conductivity is an anisotropic thermal conductivity that has a value of κ_s in the direction across the gap and zero in all other directions.

4. MODEL DESCRIPTION

The model description covers the various physics relevant to the performance of transient calculations. Section 4.1 describes the main neutronics and pebble depletion physics. Then, the thermal fluid solutions of the temperature fields needed for feedback calculations are discussed in Section 4.2. Finally, the MOOSE coupling for all physics is in Section 4.3.

4.1 Neutronics Model

A neutronics model of the HTR-PM core was developed with Griffin using an axisymmetric (R-Z) geometry with homogenized core regions. The model consists of 11 distinct regions shown in Figure 3 with the radial and axial dimensions of each region. The descriptions of the various regions and their porosity or are included in Table 9.

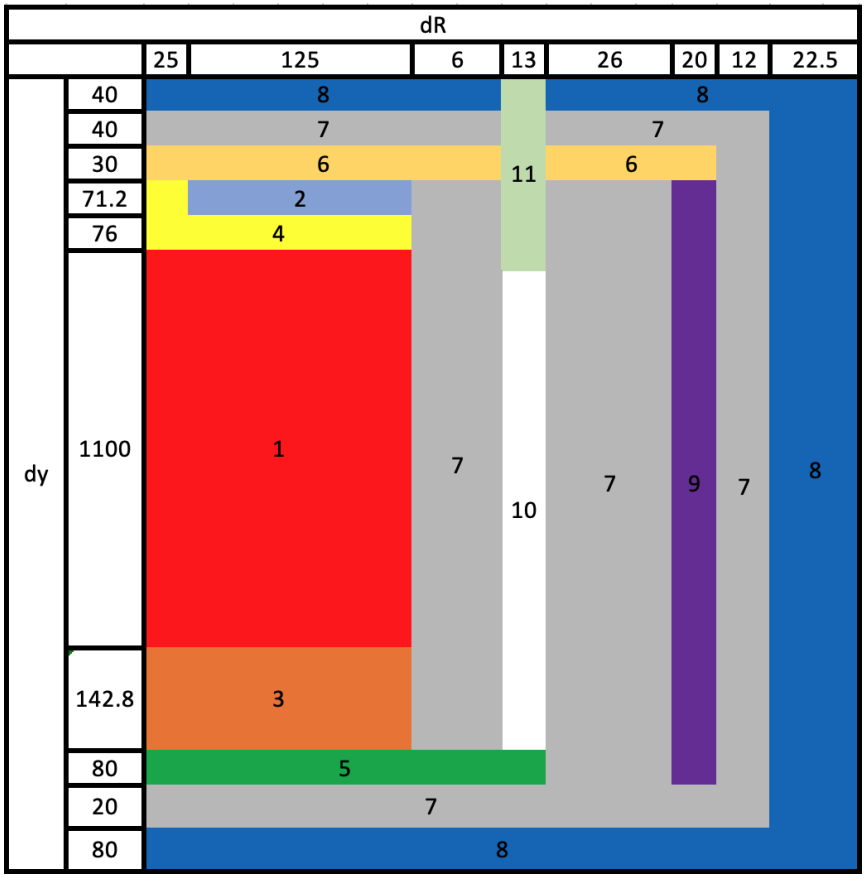

Figure 3: Geometry of the HTR-PM Griffin neutronics model, with the dimensions as the sizes of each region in centimeters.

Table 9: Explanation of the material regions in Figure 3.

Region ID	Region name	Material	Porosity
1	Pebble bed	Pebbles	0.61
2	Top reflector	Graphite	0.7
3	Bottom reflector	Graphite	0.7
4	Cavity	Helium	1.0
5	Hot plenum	Graphite	0.8
6	Cold plenum	Graphite	0.8
7	Side reflector	Graphite	1.0
8	Carbon brick	Graphite	1.0
9	Homogenized riser/side reflector	Graphite	0.68
10	Empty control rod channel	Graphite	0.72
1 1	Control rod	Graphite and boron mixture	—

The Griffin model uses six equally spaced streamlines to represent pebble depletion that are centered within the active core elements, as shown in Figure 4. The streamlines are located at radii of $r = 12.5, 37.5, 62.5, 87.5, 112.5, 137.5$ cm, representing channels whose right boundary is located at $r = 25, 50, 75, 100, 125, 150$ cm, respectively. Pebble velocity is assumed to be uniform so that the fraction of the volumetric flow rate of pebbles through each channel is proportional to the channel area. Axially the six channels are straight and begin at the bottom of the cavity and finish at the top of bottom reflector (lower conus is not simulated in the model). With the exception of the detailed fuel composition, the neutronics characteristics of the fuel are adopted from Reference [4]. Using fuel with heavy metal loading of 7 g per pebble discharging it at an average burnup of 90 MWd/kg and buring it with an average power density of 3.215 MW/m^3 (250 MW over a core volume of $V_c = \pi \times 1.5^2 \times 11 = 77.8$ m^3), and a packing fraction of 0.61, the total irradiation time in the core is estimated to be 1,055 days. 1,055 days corresponds to an average 70 days per pass in the 15-pass core design. The pebble speed of 15.6 cm/d can be calculated from the residence time per pass and the core height. Using the pebble speed the packing fraction and the pebble bed cross sectional area a pebble reloading rate of 5,949 pebbles per day is computed. The discharge burnup of 90 MWd/kg is converted to 4.82×10^{14} J/m^3 using the heavy metal density per pebble volume of 61.9 kg/m^3. A total of 10 burnup groups form the base discretization of the burnup variable was used. The first nine groups have a width of 5.35×10^{13} J/m^3 (10 MWd/kg), covering the burnup up to the average discharge limit of 4.82×10^{14} J/m^3, the last burnup group contains all discharge burnups. A summary of the streamline depletion specifications and the characteristics

of the fuel are included in Table 10 and Table 11, respectively.

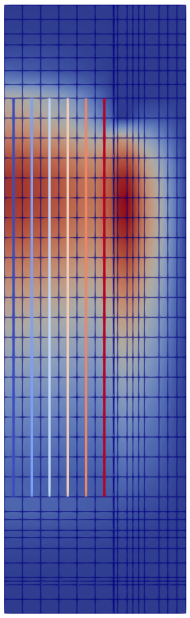

Figure 4: Overlay of the HTR-PM neutronics mesh (showing the last thermal flux group) and streamlines.

Table 10: HTR-PM model streamline depletion specifications.

Parameter	Value
Number of streamlines	6 (equally spaced)
Number of pebble types	1
Number of burnup groups	10 (from 0-100 at 10 MWd/kgU intervals)
Discharge burnup [MWd/kgU, J/m^3]	90, 4.82×10^{14}
Number of burnup groups (base)	10
Base discretization $\Delta\tau_b$ [J/m^3]	5.35×10^{13}
Pebble speed [cm/day]	15.6
Pebble unloading rate [pebbles/day]	5,949

Table 11: HTR-PM pebble composition.

Isotope	Atom Density [1/barn·cm]
U-234	1.09×10^{-7}
U-235	1.36×10^{-5}
U-238	1.42×10^{-4}
O-16	3.11×10^{-4}
O-17	1.18×10^{-7}
Graphite	8.54×10^{-2}
Si-28	3.14×10^{-4}
Si-29	1.59×10^{-5}
Si-30	1.05×10^{-5}
C-12	3.40×10^{-4}

4.2 Thermal-Hydraulics Model

The thermal-hydraulics model for Pronghorn is based on ongoing NEAMS work [25–27] with some additional improvements. The main difference from the Pronghorn model reported in Reference [26] is that the weakly compressible finite volume formulation is used for discretizing the fluid mass, fluid momentum, fluid energy, and solid energy conservation equations reported here in this work. The equations are described in detail in Reference [23]. Additional changes to the model in Reference [26] include:

- Adding a riser and bypass flow channel
- Modeling the fueling chute as an open flow region
- Reparameterizing many regions with values and correlations as shown in Table 12.

A detailed depiction of the geometry and materials in the Pronghorn thermal-hydraulics model and the fluid flow path is shown in Figure 5. In this model, the cold fluid from the circulators enters the core via the vertical risers in the reflector region. The flow then enters the cold plenum, where the flow is diverted into the cavity, upper reflector, and control and shutdown system bypass channels. From the upper cavity, the fluid enters the active core region, then the lower reflector, and finally the outlet plenum. Detailed explanations of the parameters and correlations used in each region are compiled in Table 12.

The boundary conditions for the Pronghorn thermal-hydraulics model of the HTR-PM include:

- The inlet helium flow rate is set to 96.0 kg/s

- The inlet fluid temperature is set to 523.15 K
- The outlet fluid pressure is set to 7.0×10^6 Pa
- Velocity inlet, pressure outlet, slip-wall, and symmetry boundary conditions are used for the fluid mass, momentum, and energy equations
- All walls are assumed to be adiabatic for the fluid energy equation, and conjugate heat transfer is treated as a volumetric phenomenon
- The solid energy equations have adiabatic boundary conditions except for the outside of the pressure vessel
- Radiative and convective boundary conditions were applied between the pressure vessel and isothermal cylindrical reactor cavity cooling system (RCCS) panel with an inner diameter of 4 m, a temperature of $T_\infty = 300$ K, a heat transfer coefficient of 5 $\mathrm{W/m^2K}$, and surface emissivities are assumed to be 0.8.

The radiative boundary condition at the outer boundary of the reactor vessel has a small impact on steady-state calculations and a larger impact during the loss of forced cooling transients [28]. Also, during the loss of flow transient, fluid inflow and outflow boundary conditions are not changed therefore the inventory of the helium in the core can change based on the helium temperature.

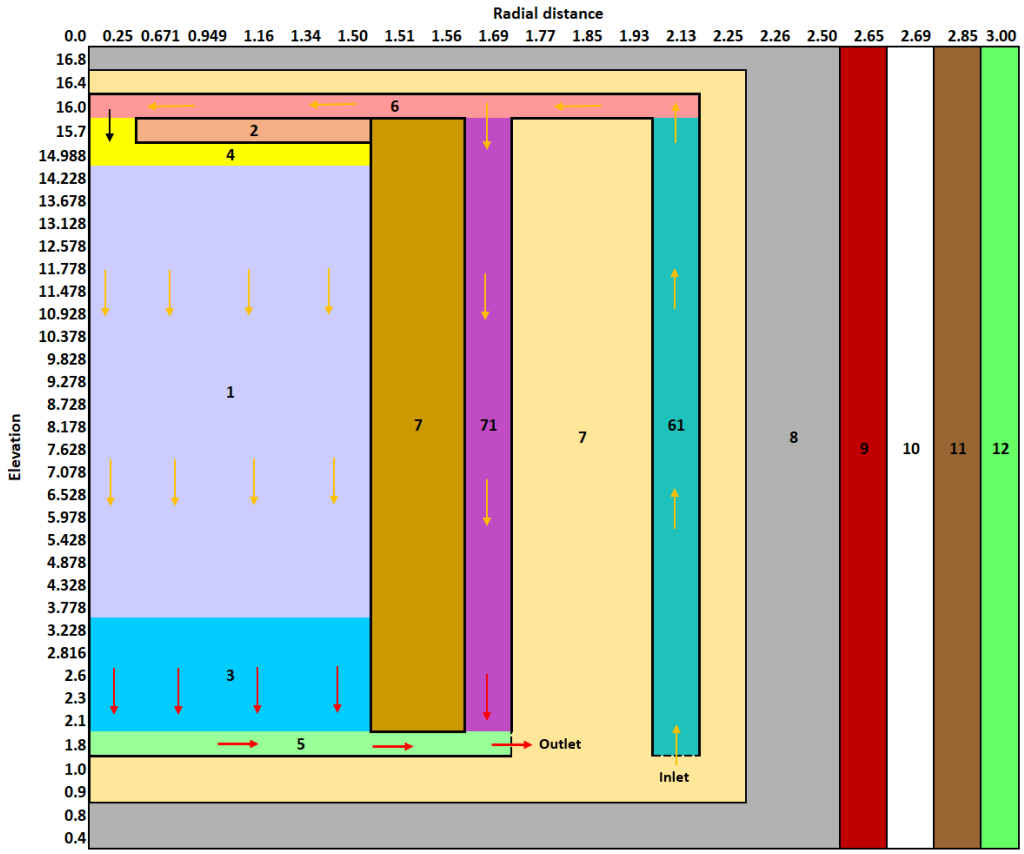

Figure 5: Thermal-hydraulics domain of the HTR-PM reference plant, where the fluid flow domain is indicated by arrows.

ID	Name	Porosity ϵ	D_H	κ_s	κ_f	Drag	α
1	Pebble bed	0.39	0.06	k_s^a	linear Peclet model	KTA	Wakao PBR correlation
2	Top reflector	0.3	0.2	$k_{Gr}(1-\epsilon)$	k_f	Churchill†	D-T
3	Bottom reflector	0.3	0.2	$k_{Gr}(1-\epsilon)$	k_f	Churchill†	—
4	Top cavity	1	0.67	—	Gap model	—	—
5	Hot plenum*	0.2	1	$k_{Gr}(1-\epsilon)$	k_f	$F = 0.063$	5×10^3W/m^3-K
6	Cold plenum*	0.2	1	$k_{Gr}(1-\epsilon)$	k_f	$F = 0.063$	5×10^3W/m^3-K
7	Side reflector	0	—	k_{Gr}	—	—	—
8	Carbon brick	0	—	k_{Gr}	—	—	—
9 & 11	Gas gap	0	—	Gap model	—	—	—
10	Core barrel	0	—	$k_s = 17$W/m-K	—	—	—
11	Reactor pressure vessel	0	—	$k_s = 38$W/m-K	—	—	—
61	Riser	0.32	0.1875	$k_{Gr}(1-\epsilon)$	k_f	Churchill	D-T
71	Bypass channel	0.32	0.15	$k_{Gr}(1-\epsilon)$	k_f	Adjusted	D-T

k_s^a Radiation: Breitbach-Barthels, Conduction: ZBS, Fluid conduction: ZBS
$k_{Gr} = 26$ W/m-K is the assumed thermal conductivity of graphite
k_f is the molecular thermal conductivity of helium
† Churchill correlation in the vertical direction, very large pressure drop coefficient in the radial direction
D-T is the Dittus-Boelter heat transfer correlation converted to a volumetric heat transfer coefficient
Gap model: the effective conductivity in gaps is defined in Section 2.2.1 in Reference [25]
* The authors do not have reliable information for the hot and cold plenum so the selected parameters are likely unrealistic
Drag coefficient in the bypass channel is adjusted to yield a mass flow rate of 1 kg/s

Table 12: Modeling parameters and closure relations used in the Pronghorn HTR-PM reference plant model, where D_H is the characteristic length of each region in m, κ_s is the effective solid thermal conductivity, κ_f is the effective fluid thermal conductivity, α is the volumetric heat transfer coefficient, and F is the Forchheimer coefficient. Regions with a porosity of zero have no defined flow variable.

4.3 Equilibrium Core Coupled Model

The developed HTR-PM reference plant model for equilibrium core multiphysics calculations in this work consists of a MOOSE main application (*mainApp*) and two multiphysics applications (*multiApps*), which can spawn a number of subapplications (*subApps*). The setup for the coupled model is in Figure 6. *mainApp* solves the neutronics problem within Griffin, which includes the steady-state neutronics calculations and streamline depletion-advection problem, and establishes the transfer system to exchange coupling variables between *mainApp* and *multiApps*. The first *multiApps* (MA1) solves the thermal fluid problem with Pronghorn in a single *subApps*. The second *multiApps* (MA2) solves the pebble and TRISO conduction problem in 1,200 *subApps*, representing each pebble type and burnup group in each active core region.

The coupling variable transferred within the *mainApp* and between *mainApp* and *multiApps* are:

- The scaled neutron flux (within *mainApp*): to compute the reaction rates and perform the 1D depletion-advection calculations
- Number densities and volume fractions for each pebble type and burnup group (within *mainApp*): to reconstruct the cross sections in each reactor region
- Power density (*mainApp* $\rightarrow$ MA1): to compute the heat source for the thermal fluids calculations
- Pebble surface temperature and reflector temperature (MA1 $\rightarrow$ *mainApp*): to provide all solid temperatures to Griffin to call the pebble and TRISO *multiApps* and interpolate all cross sections outside the pebble bed
- Pebble surface temperature and fractional power density for each pebble type and burnup group (*mainApp* $\rightarrow$ MA2): to provide the boundary conduction for the pebble problem and the heat source for the pebble and TRISO conduction
- Fuel and moderator temperatures (MA2 $\rightarrow$ *mainApp*): to provide all temperatures to interpolate the cross sections for the pebble bed.

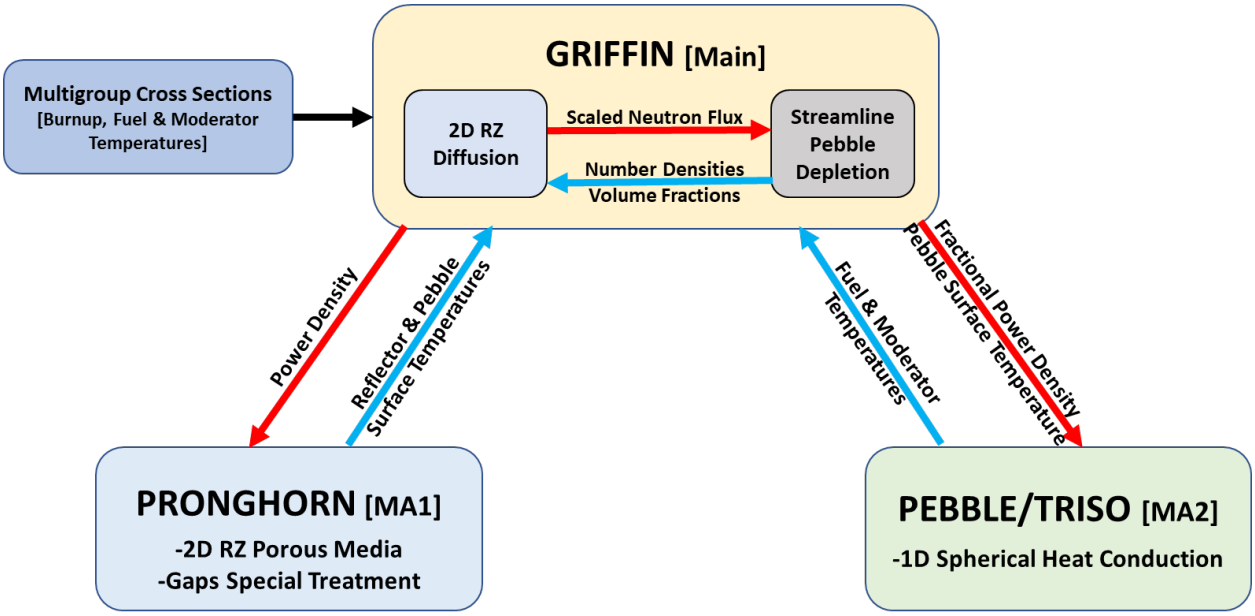

Figure 6: Coupling scheme of the equilibrium core multiphysics calculations of the HTR-PM using Griffin, Pronghorn, and MOOSE.

4.4 Assumptions and Limitations

The following assumption and limitations are applicable to the developed neutronics model:

1. A 2D RZ representation of the reactor core is used, and is a good representation of the reactor geometry.

2. The multigroup neutron diffusion equation provide a flux solution for the core and reflector regions accurate enough for equilibrium core calculations.

3. The grey curtain model developed to model the control rods is not corrected using SPH equivalence since is not available for equilibrium core calculations. The deployment of a fast SN solver is planned for future work to better reproduce the effect of the control rods.

4. The multigroup cross sections are prepared using an infinite, reflected domain in the lattice physics calculation. The intra-core neutron leakage affects the local spectrum significantly and will have an impact on the cross-section homogenization [29]. Nevertheless, these serve as an initial set to perform preliminary calculations until more sophisticated methods are available in Griffin.

5. A flux-limited approximation of the isotope transport cross sections is sufficient to build acceptable diffusion coefficients for this reactor.

6. The cumulative migration method provides accurate diffusion coefficients for the void regions in the top plenum, but they are not currently temperature dependent.

7. A 1D streamline depletion is sufficient to capture the pebble flow since experiments show that the flow is axially dominated [30].

The assumptions and limitations applicable to the developed thermal fluids model are that:

1. Porous medium equations capture most of the important effects in the core

2. The flow in the plena is approximated for lack of detailed information about the geometry and will require either empirical or CFD-computed closure models to be further improved, but is not expected to change the core temperatures results significantly.

3. Wall effects for convection, radiation, and conduction heat transfer are approximated not explicitly treated

4. There is no convective heat transfer between the fluid and reflector regions, so only conduction was considered

5. Slip-wall, and symmetry boundary conditions are used for the fluid mass, momentum, and energy equations.

6. All walls are assumed to be adiabatic, and the conjugate heat transfer is treated as a volumetric phenomenon

7. The solid energy equation boundaries are all adiabatic except for the outside of the pressure vessel

8. Radiative and convective boundary conditions were applied between the RPV and the RCCS.

9. RCCS temperature is constant and is set to 70 ^{o}C.

The following assumptions are applicable to the developed pebble and TRISO thermal model:

1. Thermal equilibrium approximation was considered in pebble simulations during transient calculations, thus using the quasi-static approximation in the pebble and TRISO thermal conduction problem is acceptable for slow transients since the two will be in thermal equilibrium, and the Pronghorn solid conduction solution already includes the time-dependent term to compute the surface temperature

2. Several sources of heat transfer heterogeneity around the pebble were ignored: the coolant flow orientation, pebble-to-pebble contact, pebble-to-reflector contact, and radiation.

3. A Dirichlet boundary condition is set at the pebble surface to obtain the moderator temperature, and a Robin boundary condition that couples directly to the fluid temperature via the heat transfer coefficient would improve energy conservation.

4. A Dirichlet boundary condition is set at the TRISO surface to obtain the fuel temperature, and a Neumann boundary condition would improve energy conservation.

5. The thermophysical properties for the fuel kernel are based on UO_2 data, so ideally, we would need to use uranium oxycarbide data.

5. RESULTS

The results of the equilibrium core calculations and transient analysis are discussed in this section and verified against available VSOP (very superior old programs) solutions from open literature. Section 5.1 discusses the cross sections generated with infinite homogeneous medium approximations are audited to ensure that all values are within acceptable limits. Section 5.2 presents the equilibrium core calculations are performed for the HTR-PM reference plant model. In Section 5.3, the DLOFC transient scenario results are presented.

5.1 Cross Section Audit

A comparison of the DRAGON depletion for a single pebble and pebble ensemble with neighboring pebbles at the MOL is shown in Figure 7 considering the infinite multiplication factor (k_{inf}) and burnup. The microscopic cross-section tabulations are obtained with the results from the nominal depletion of the pebble ensemble. Changes in the k_{inf} in the pebble ensemble are small due to only the central pebble of interest being depleted.

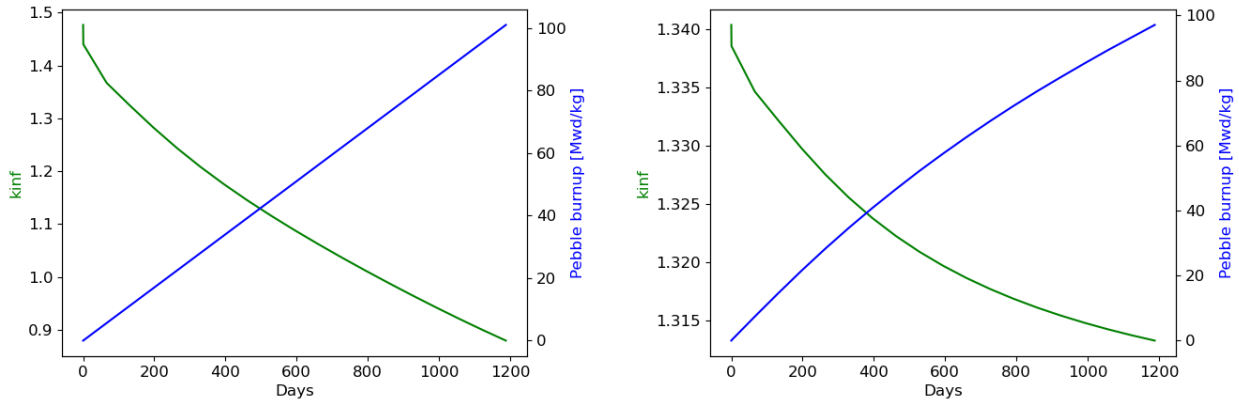

(a) Pebble

(b) Ensemble

Figure 7: Comparison of the DRAGON pebble and ensemble depletion.

We performed an isothermal temperature coefficient (ITC) check in an infinite homogeneous domain with Griffin in order to verify some of the feedback characteristics of the cross-section tabulation, as shown in Figure 8. For all cases, the ITC values are all negative with expected magnitudes. The calculations were performed with isothermal temperatures in the range from

500 to 2000 K. The ITC values are ranging between -1.0 and -12.0 pcm/K, and its magnitude is monotonically decreasing with temperature except for the BOL case.

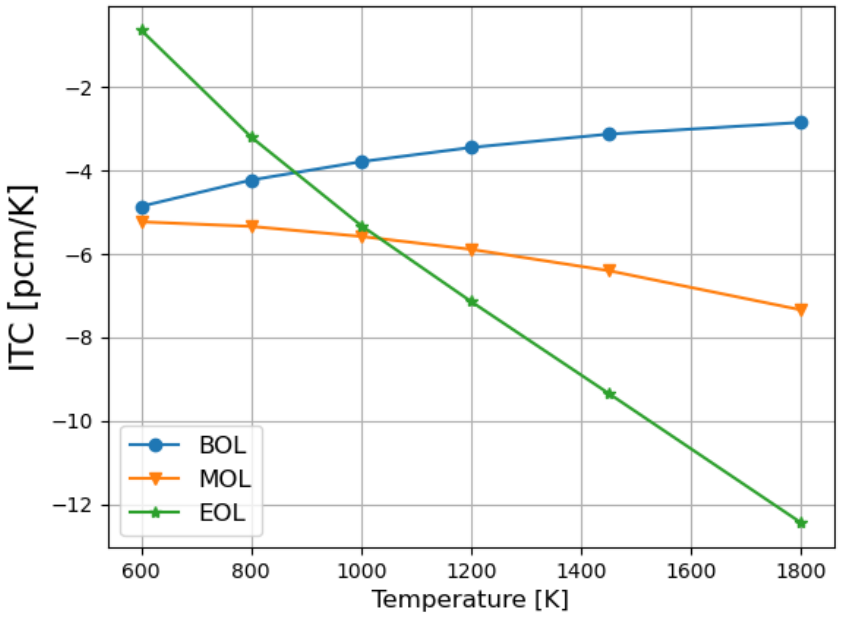

Figure 8: ITCs of reactivity for an infinite homogeneous domain.

5.2 Equilibrium Core

This section presents the steady-state equilibrium core calculation results of the HTR-PM reference plant model. The steady-state global parameter values for the equilibrium core calculation results are shown in Table 13 and compared to VSOP considering eigenvalue, peak power, power density, average and maximum fuel temperatures, temperature coefficients, and kinetics parameters. Compared to VSOP results, most of the parameters are in good agreement with the reference solutions, and the discrepancies are mainly attributed to differences in the discretization methods, multigroup cross section generation, and lack of information on the VSOP models. The VSOP eigenvalue was not reported, so it was assumed critical. The peak power density and power ratio are in very good agreement with the VSOP results. Differences of respectively 40 and 20 K were observed in the maximum and average fuel temperatures, mainly due to differences in the discretization methods and the material properties.

Also, a comparison of the temperature coefficients of reactivity for the equilibrium core is pro-

Table 13: Nuclear parameters of equilibrium core, with a discharge burnup 90 MWd/kgU.

Parameter	Unit	Griffin	VSOP
k_{eff}	—	0.9958	1.0000 (assumed)
Power peak	—	2.00	2.04
Peak power density	MW/m^3	6.40	6.56
Average core burnup	MWd/kgU	53.62	—
Maximum fuel temperature	K	1124.6	1163.2
Average fuel temperature	K	899.0	873.2
Average moderator temperature	K	886.0	—
Average fluid temperature	K	653.0	—
Fuel temperature coefficient	pcm/K	-4.32	-4.36
Moderator temperature coefficient	pcm/K	-1.92	-0.94
Reflector temperature coefficient	pcm/K	0.72	1.49
Λ	s	0.0013	0.0011
β_{eff}	pcm	519.0	549.0

vided in Table 13. The temperature coefficients were calculated by perturbing the temperature of the fuel, moderator, or reflector by $\pm$50 K, as shown in Figure 9. The results show that the fuel temperature coefficient is consistent with the reported value from VSOP. Both the moderator and reflector coefficients, which depend primarily on graphite scattering, are different between the codes due to the use of different libraries. The graphite cross sections in ENDF/B-VIII.r0 is significantly different from that in other evaluations. Also, the kinetics parameters were compared, and both the mean generation time (Λ) and effective delayed neutron fraction are consistent with the VSOP values. The kinetic parameters were obtained with the Improved Quasi-Static (IQS) method in Griffin, and the values of each delayed neutron group are included in Table 14 for effective delayed neutron fractions and decay constants.

Table 14: Kinetic parameters for the equilibrium core calculated by Griffin.

Precursor Group	1	2	3	4	5	6
$\beta[pcm]$	17.34	99.26	88.35	194.7	85.46	33.73
$\lambda[s^{-1}]$	0.01334	0.03274	0.12078	0.30278	0.8495	2.853

Also, Figure 10 shows the distributions of the important neutronics parameters in the reactor core region, including isotopic distributions of ^{235}U and ^{239}Pu and distributions of the total, decay, and peak powers. Figure 11 shows the distributions of the important thermal hydraulics

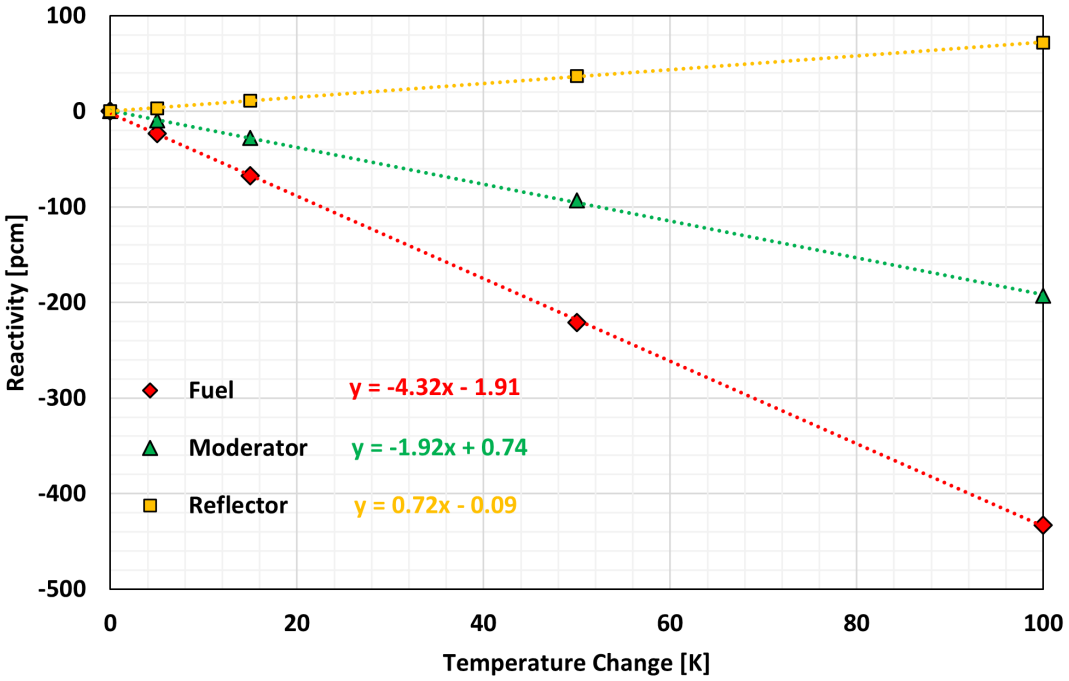

Figure 9: HTR-PM equilibrium core temperature coefficients.

parameters, including fluid and solid temperatures, axial velocity field, and pressure field. The solutions of the field variables are as expected. The power peaks skewed to the upper core region or high in the center of the core, where the fluid and solid temperatures are significantly lower compared to the bottom core region and the control rod is partially inserted into the upper core region. Also, the concentrations of ^{235}U are high at the top core region due to loading the fresh pebbles from the top of the core region, while the ^{239}Pu concentrations show the opposite behavior due to producing ^{239}Pu from the neutron capture reaction in ^{238}U and its accumulation with burnup.

Both the fluid and solid temperature (the pebble surface temperature in the bed) peak at the center-bottom of the pebble bed. Both the top and side reflectors are relatively cool, while the bottom reflector is hot but cooler than the bottom of the bed as the heat exchange between the fluid and solid is not simulated in that region and some heat is removed trough the bottom of the vessel. Flow comes up the riser, enters the cold plenum, and distributes between the bypass core channel and pebble bed. In the bed, the flow velocity is almost uniform in the radial direction, but it increases from top to bottom because the gas density lowers as it traverses the bed.

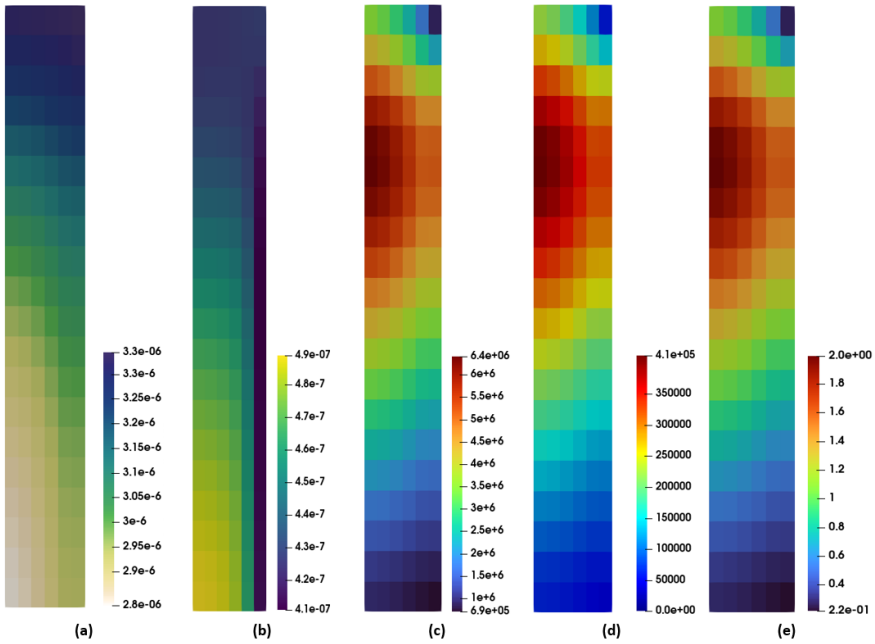

Figure 10: BlueCRAB equilibrium core neutronic distributions of (a) ^{235}U, (b) ^{239}Pu, (c) power density, (d) decay power density, and (e) power peaking.

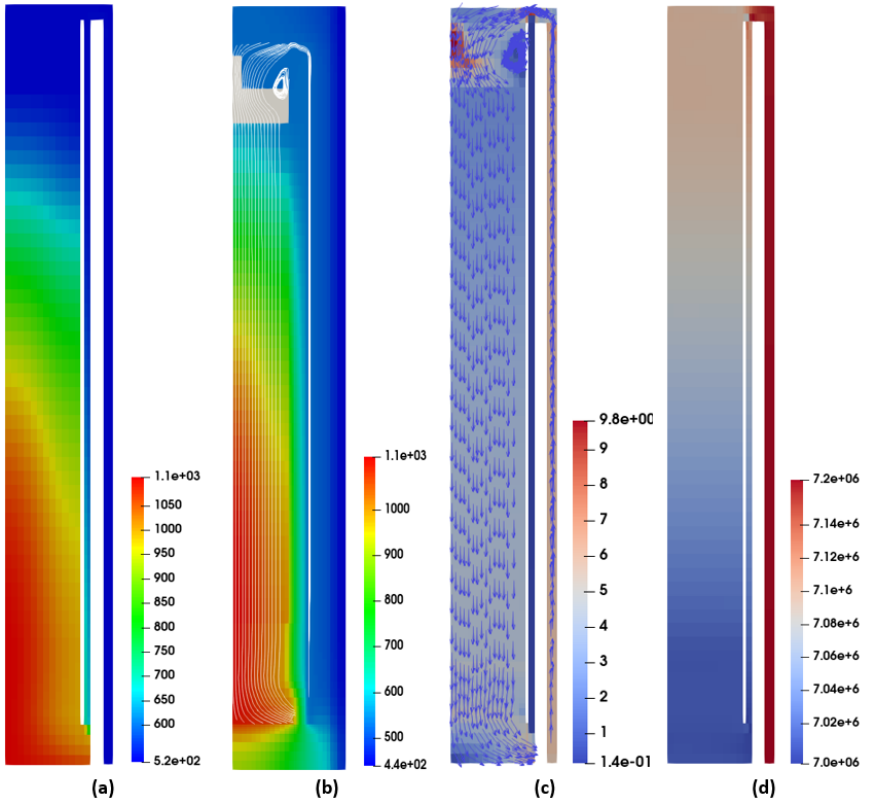

Figure 11: BlueCRAB equilibrium core thermal fluid distributions of (a) fluid temperature, (b) solid temperature, (c) superficial velocity magnitude, and (d) pressure.

5.3 Depressurized Loss Of Forced Cooling Transient

The DLOFC is one of the most challenging design basis accidents because it assumes that the coolant completely leaked out of the RPV. In this accident, a large break in the main coolant flow pipe was assumed, resulting in a fast reduction of the helium inventory in the system followed by a depressurization of the reactor. The natural circulation effect has a minimal contribution to the heat extraction from the fuel due to the low coolant density at atmospheric pressure. Instead, the heat will be extracted from the fuel trough conduction and radiation, through the reflector the barrel the RPV and the RCCS. It is important to show that the maximum fuel temperature is not exceeding the safety limits and the reactor is able to remove the heat efficiently. The results of the protected DLOFC transient simulation for the HTR-PM equilibrium core are presented in this section.

The DLOFC transient simulation was initiated by reducing the mass flow rate of the coolant from its nominal value to zero over thirteen seconds. At the same time, the system pressure was reduced from 7.0 MPa to atmospheric pressure (0.101 MPa), assuming these changes will behave linearly and that the DLOFC transient is a protected transient. Therefore, after the initiation of the accident, the control rods were fully inserted (SCRAM) to shutdown the reactor after completing the flow rate and pressure ramps. Beyond that, there were no changes to the system's main parameters, and the simulation was performed for up to 140 hours. The sequence of events for the DLOFC transient is listed in Table 15 and the change in the helium mass flow rate and average temperature across the core are shown in Figure 12 during the first 50 s of the DLOFC accident.

During the DLOFC transient simulation, coupled neutronics and thermal-hydraulics calculations were performed at each time step to obtain the time-dependent power density distribution in the pebble-bed region, including the decay heat, which is the main driving heat source during the transient as the prompt power goes to zero after control rod insertion. The evolution of the reactor's total power and the maximum and average fuel temperatures during the DLOFC accident are shown in Figure 13. The following progression of the reactor power was observed during the transient:

- The reactor power starts decreasing at the beginning of the transient due to the negative thermal feedback as the fuel and moderator temperatures increase following the helium

flow rate reduction in the system

- At around t = 15 seconds, a large reduction in the reactor power can be noticed as the control rods are fully inserted to shut down the reactor
- Beyond that point, the prompt power goes to zero while the remaining reactor power is just the decay heat component of the fuel.

The fuel temperature increases at a lower rate and attains its maximum value around 20 hours after the start of the transient. The fluid and solid (surface pebble) temperature distributions at different time steps of the transient are provided in Figures 14 and 15, respectively. Also, the temperatures of the bed's outer regions as a function of time are shown in Figure 16 and 17, along with the RPV heat loss rate. The following progression of the reactor temperatures was observed during the transient:

- During steady-state operation (t = 0), the fluid and solid temperatures peak at the center-bottom of the pebble bed. The reflector temperature is higher at the bottom region, rather than the radial and top reflectors, which are much cooler.
- From t = 0–14 hours, the maximum fluid and solid temperatures start moving axially and toward the top of the core. This is caused by the decay heat distribution, which peaks towards the top of the core.
- Beyond t = 14 hours, the fluid and solid temperature distributions within the core region change very slowly.
- Temperature distributions change mainly in the radial direction, and there is a significant change in the solid temperature of the reflector and RPV regions. The RPV peak temperature happens at about hour 100 of the transient, which is significantly after bed temperature peak (around 20 hours).
- The heat loss rate from the RPV peaks (1,000 kW) at around hour 100 of the transient and starts decreasing gradually after that.

Table 15: Sequence of events for the protected DLOFC.

Time [s]	Event
< 0	Equilibrium steady state completed
0	Start of accident
0–13	Start linearly reducing outlet pressure to 0.1 MPa over 13 s Start linearly reducing mass flow rate to 0 kg/s over 13 s
13	Mass flow rate and pressure ramps completed Initiate SCRAM
13–16	Fully insert control rods
16	SCRAM completed Power level is determined by decay heat until end time
360,000	Simulation end time

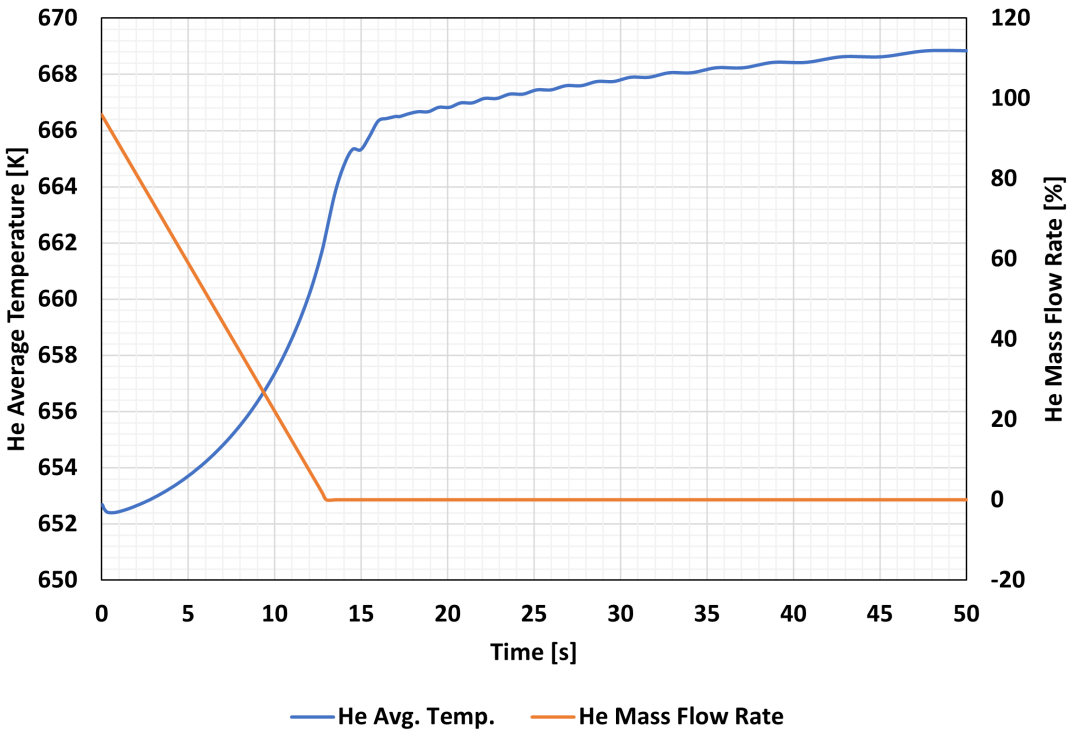

Figure 12: Change in helium mass flow rate and helium average temperature across the core during the first 50 s of the DLOFC accident.

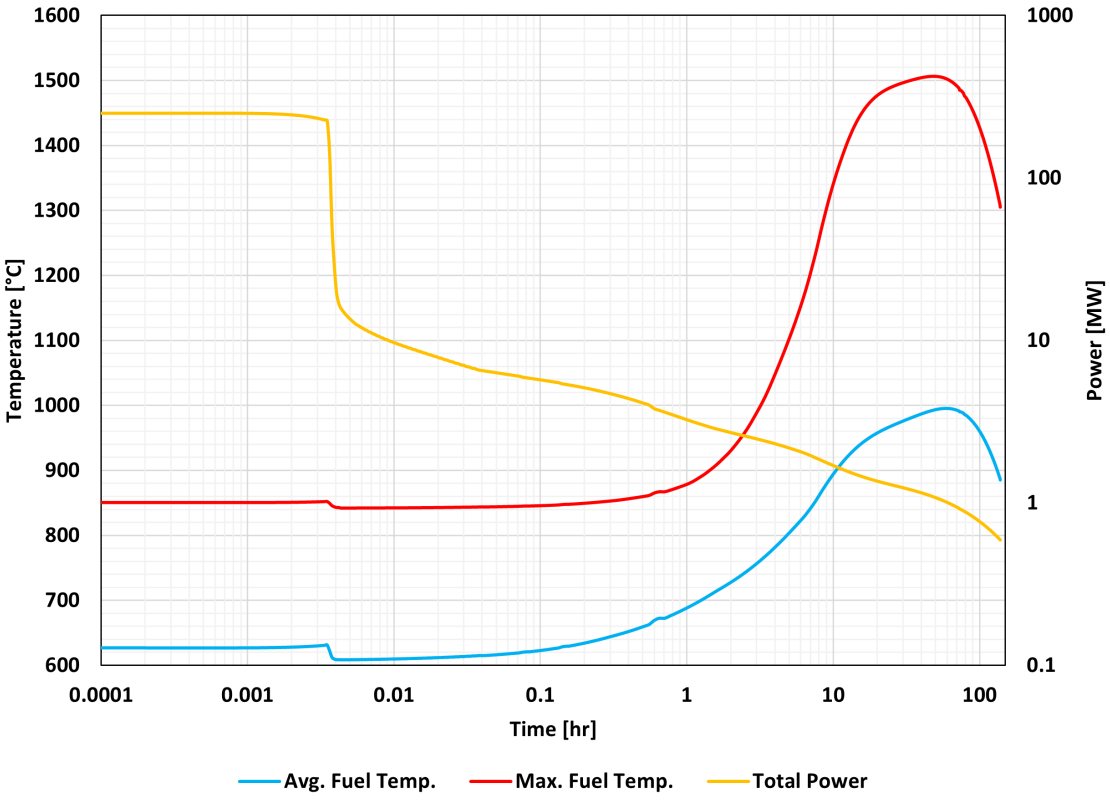

Figure 13: Power and temperature evolution during a DLOFC accident.

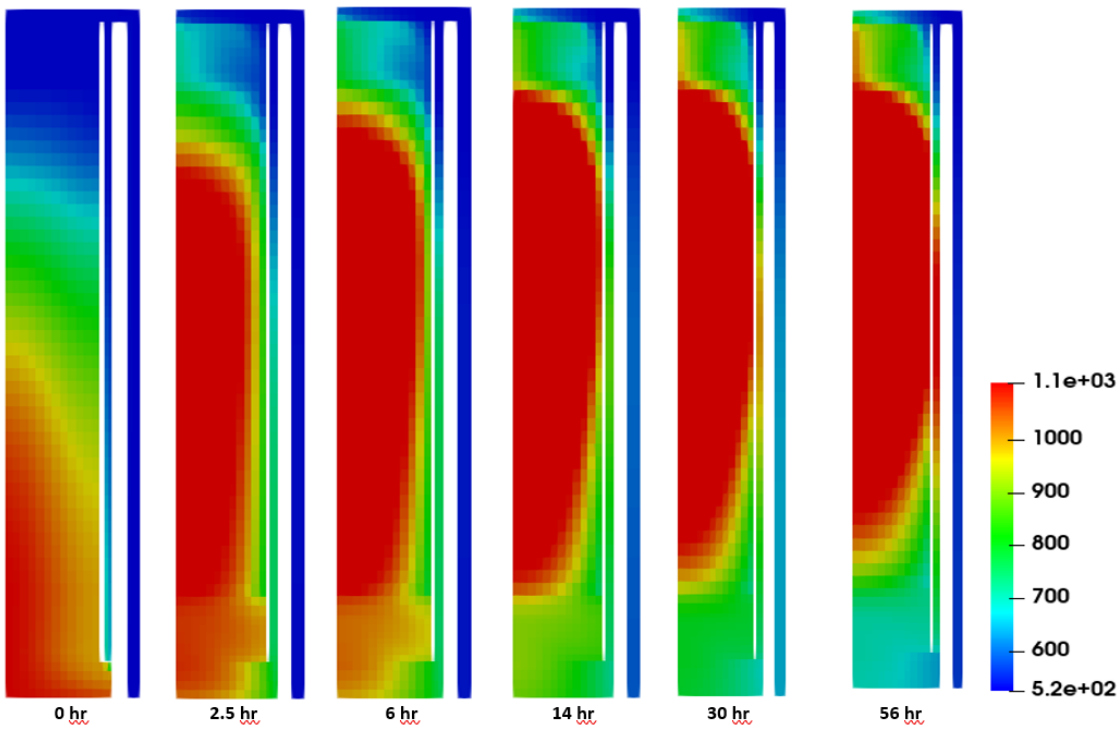

Figure 14: Fluid temperature distribution as function of time during a DLOFC accident.

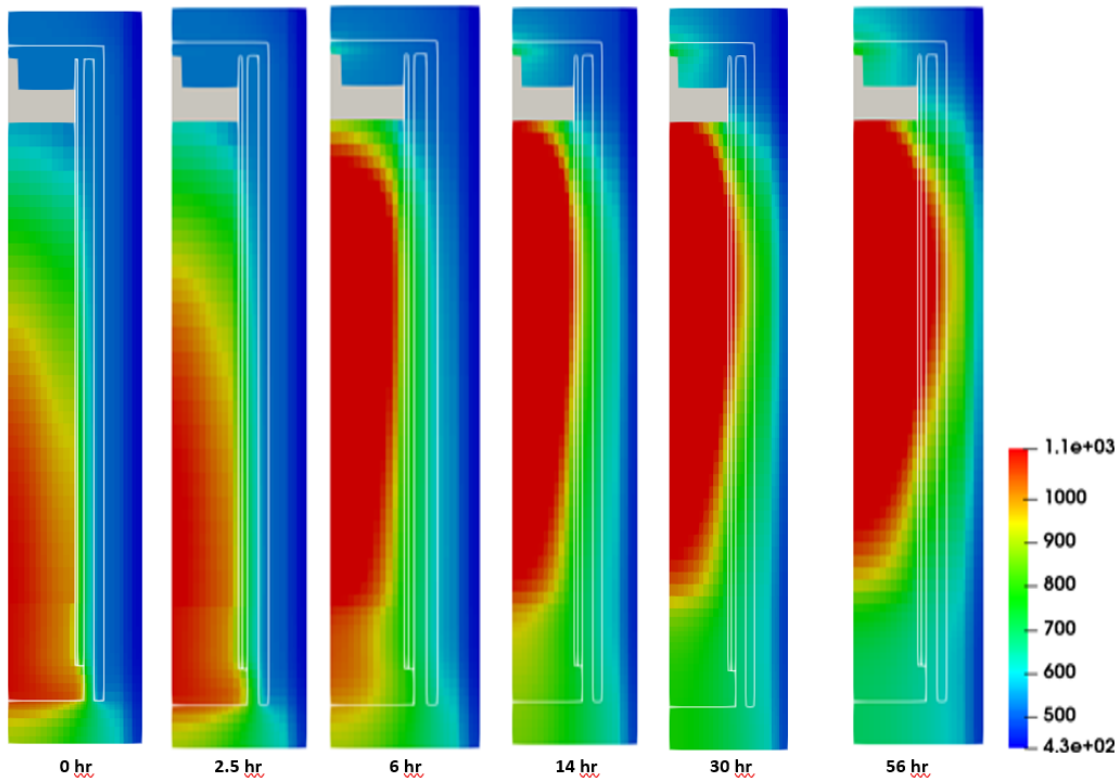

Figure 15: Solid temperature distribution as function of time during a DLOFC accident.

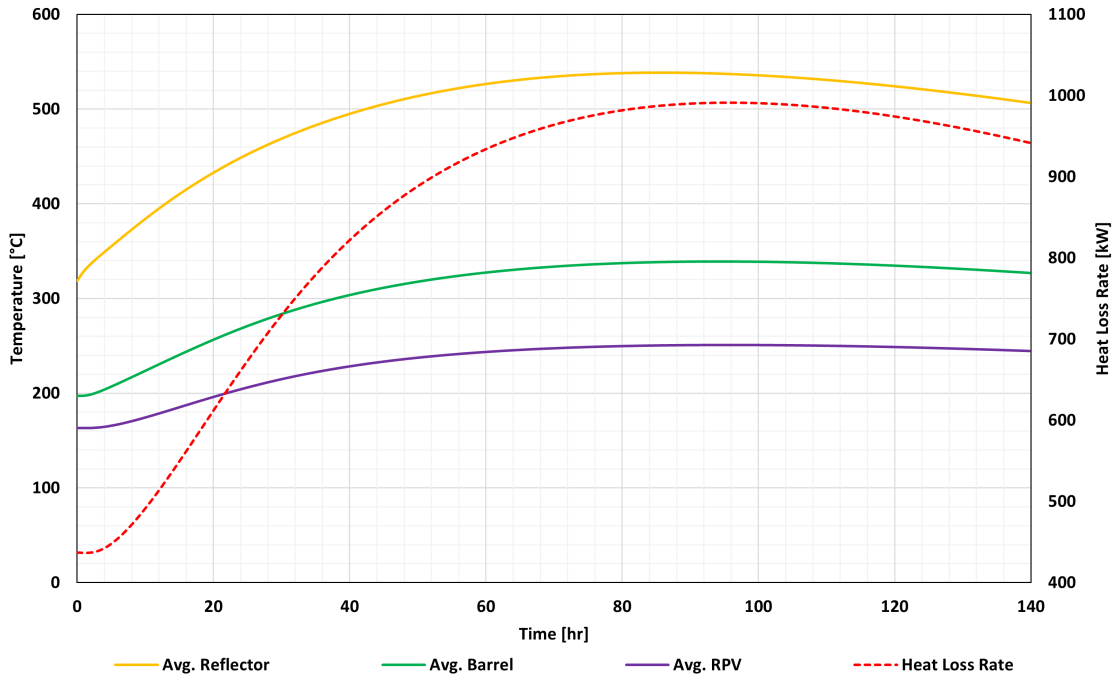

Figure 16: Average Temperature evolution of outer core regions during a DLOFC accident.

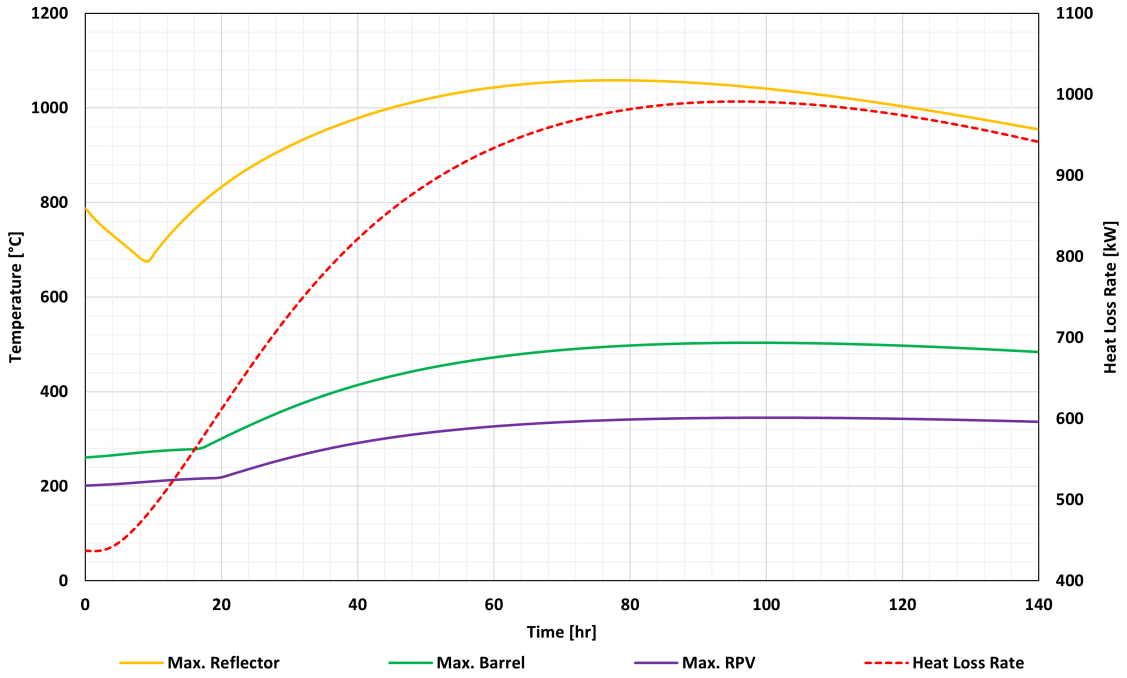

Figure 17: Maximum Temperature evolution of outer core regions during a DLOFC accident.

To verify the DLOFC transient results, a one-to-one comparison of the average and maximum fuel temperatures, barrel and RPV maximum temperatures, and RPV heat loss rate against VSOP

results of the DLOFC, as shown in Figures 18, 19, and 20. The reference VSOP solutions were obtained from open literature and were digitized for direct comparison. Also, Table 16 provides VSOP and BlueCRAB solutions for the maximum and average temperatures of the fuel, barrel, and RPV and the maximum heat loss rates. The following progression was observed during the transient compared to the VSOP solution:

- Up to t = 30 hours, the fuel average and maximum temperatures match very well with the reference solution and a peak maximum and average values of 1506.2^{o}C and 995.2^{o}C, respectively, with a difference of about 15^{o}C from the reference solution.
- Beyond t = 30 hours, the solutions behave similarly with higher fuel temperatures obtained by BlueCRAB.
- The maximum barrel and RPV temperatures, as well as the RPV heat loss rate agree in shape with the reference solution, while the magnitude is slightly higher.

The differences between the BlueCRAB and VSOP solutions can be attributed to the differences that exist between the neutronics and thermal hydraulics models of each solution. These differences can be summarized as:

- The discretization methods of the neutronics codes.
- Multigroup cross sections: VSOP uses online cross sections, while Griffin uses a two-step process that does not satisfactorily treat leakage effects in the core. Also, the broad energy group structures are different.
- Uncertainties regarding the VSOP model: the control rods position is unknown, the neutronics geometry was not reported in the reference, and the detailed composition of all neutronics regions was not provided.
- The Pronghorn model doesn't include the cold leg, which cools the bottom reflector in the VSOP model.
- The Pronghorn model uses the full porous flow set of equations, including advection terms in the fluid momentum equations, while VSOP uses a friction-dominated model where the advection terms in fluid momentum terms are neglected.

- Material properties of the graphite, especially thermal conductivity, are slightly different between the two models.

Table 16: Average and maximum temperatures during a DLOFC accident.

Parameter	VSOP[4]	BlueCRAB
Fuel average [^{o}C]	979.5	995.2
Fuel maximum [^{o}C]	1492.0	1506.2
Barrel average [^{o}C]	—	338.9
Barrel maximum [^{o}C]	437.8	503.4
RPV average [^{o}C]	—	251.1
RPV maximum [^{o}C]	318.0	345.3
Heat loss rate maximum [kW]	918.0	991.3

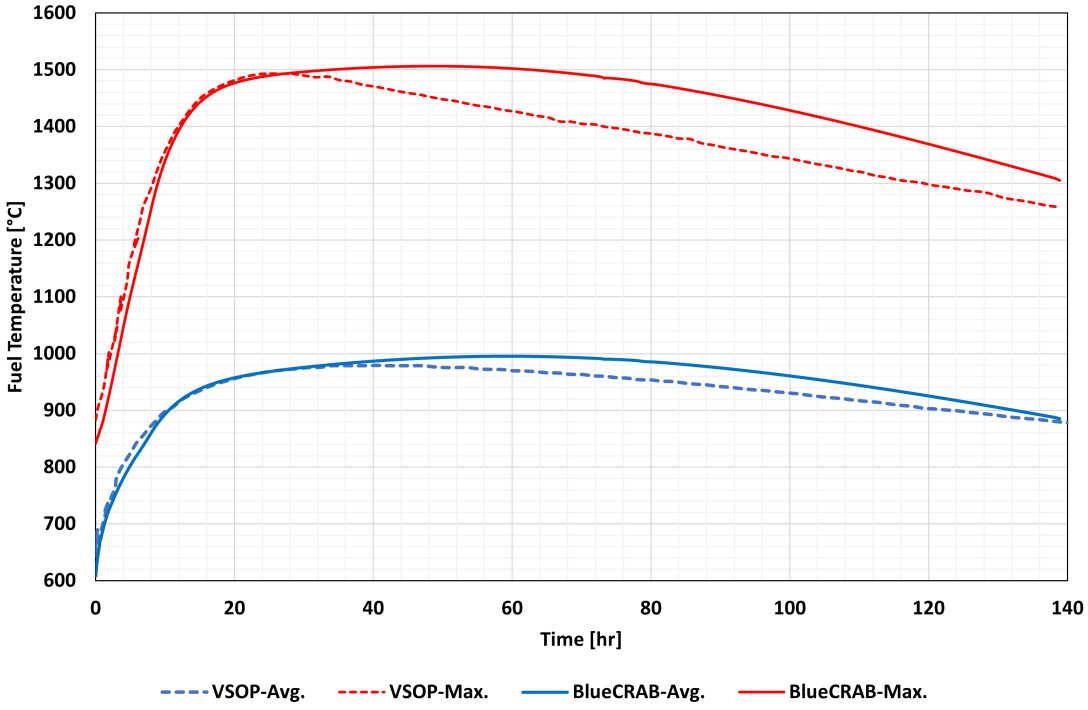

Figure 18: Comparison of average and maximum fuel temperatures during a DLOFC accident.

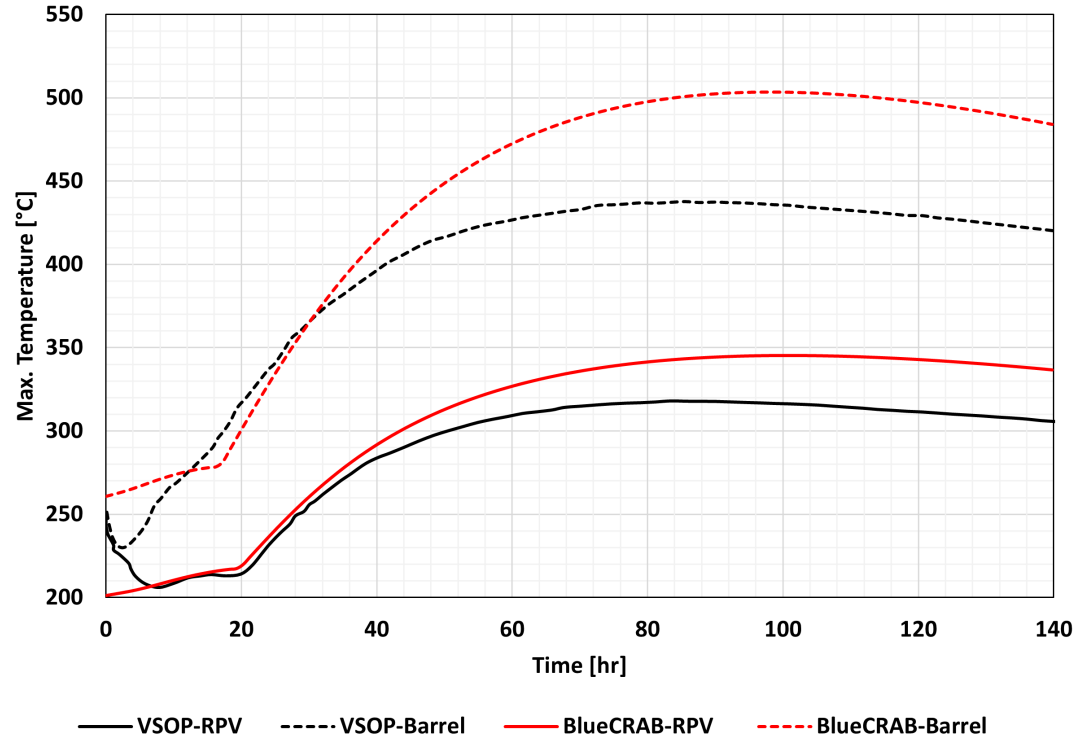

Figure 19: Maximum RPV and barrel temperatures during a DLOFC accident.

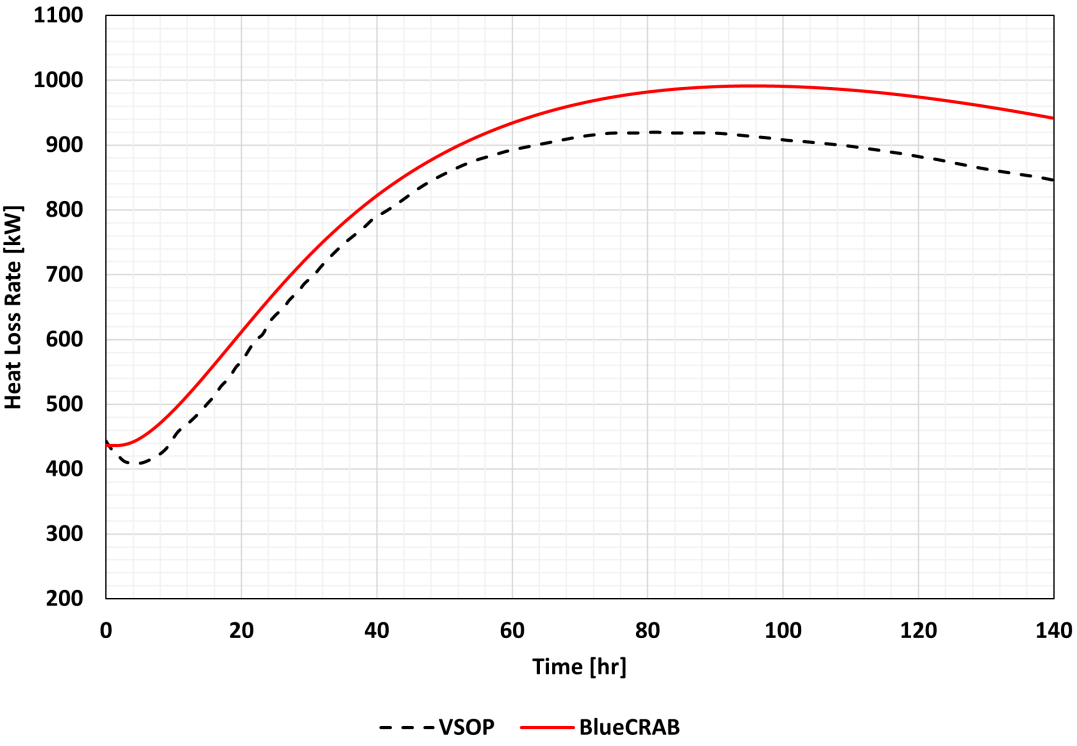

Figure 20: Heat loss rate from RPV during a DLOFC accident.

6. CONCLUSIONS

This report details INL's progress and activities for the NRC project "Development and Modeling Support for Advanced Non-Light Water Reactors" and reports the successful completion of one task, including:

- #6—DLOFC calculation for gas-cooled pebble-bed reactor.
- #15—Reference plant model for gas-cooled pebble-bed reactor (thermal spectrum).

This report demonstrates the modeling and simulation of a reference plant model for a gas-cooled pebble-bed reactor using BlueCRAB. The fully coupled neutronics and thermal hydraulics calculations models produced the steady-state solutions of the equilibrium core. The protected DLOFC accident scenario was simulated for the equilibrium core with the coupled neutronics and thermal hydraulics system. The steady-state and transient solutions of the equilibrium core were assessed against reference solutions obtained from open literature for the purpose of verification. A good agreement was observed in general for all solutions, and several sources of differences were identified between the current and reference models. Further improvements and modifications of the current model are suggested and discussed Section 7.

7. FUTURE WORK

Future work should consider the following changes to improve reactor physics:

1. Add Griffin cross-section preparation capabilities to provide online cross sections
2. Investigate the discrepancy in the moderator and reflector feedback coefficients compared to the reference
3. Deploy a transport solver instead of the diffusion solver
4. Improve the control rod model
5. Investigate a 3D representation of the core by developing an analog model in Monte Carlo
6. Add conical pebble-bed sections
7. Improve porosity distribution with a more realistic value.

Future work should consider the following changes to improve thermal fluids:

1. Improve closures to accurately model plena
2. Improve porosity distribution with a more realistic value
3. Couple the current model with a system analysis code to consider the outer loop in the transient analysis
4. Improve the RCCS model and boundary conditions applied at the outer surface of the RPV

REFERENCES

[1] "Pbmr coupled neutronics/thermal-hydraulics transient benchmark the pbmr-400 core design," Tech. Rep. Tech. Rep. NEA/NSC/DOC(2013)10, OECD/NEA, 2013.

[2] Z. Zhang, Y. Dong, F. Li, Z. Zhang, H. Wang, X. Huang, H. Li, B. Liu, X. Wu, H. Wang, X. Diao, H. Zhang, and J. Wang, "The shandong shidao bay 200 mwe high-temperature gas-cooled reactor pebble-bed module (htr-pm) demonstration power plant: An engineering and technological innovation," *Engineering*, vol. 2, pp. 112–118, 03 2016.

[3] D. Tian, L. Shi, L. Sun, Z. Zhang, Z. Zhang, and Z. Zhang, "Installation of the graphite internals in htr-pm," *Nuclear Engineering and Design*, vol. 363, p. 110585, 2020.

[4] Y. Zheng, L. Shi, and Y. Dong, "Thermohydraulic transient studies of the chinese 200mwe htr-pm for loss of forced cooling accidents," *Annals of Nuclear Energy*, vol. 36, no. 6, pp. 742–751, 2009.

[5] C. Tang, Y. Tang, J. Zhu, Y. Zou, J. Li, and X. Ni, "Design and manufacture of the fuel element for the 10 mw high temperature gas-cooled reactor," *Nuclear Engineering and Design*, vol. 218, no. 1, pp. 91–102, 2002.

[6] "Evaluation of the initial critical configuration of the HTR-10 pebble-bed reactor.," Tech. Rep. HTR10-GCR-RESR-001, International Reactor Physics Experiment Evaluation Project, 2006.

[7] Z. Wu, D. Lin, and D. Zhong, "The design features of the htr-10," *Nuclear Engineering and Design*, vol. 218, pp. 25–32, 2002.

[8] C. J. Permann, D. R. Gaston, D. Andrš, R. W. Carlsen, F. Kong, A. D. Lindsay, J. M. Miller, J. W. Peterson, A. E. Slaughter, R. H. Stogner, and R. C. Martineau, "MOOSE: Enabling massively parallel multiphysics simulation," *SoftwareX*, vol. 11, no. 10, p. 100430, 2020.

[9] D. R. Gaston, C. J. Permann, J. W. Peterson, A. E. Slaughter, D. Andrs, Y. Wang, M. P. Short, D. M. Perez, M. R. Tonks, J. Ortensi, L. Zou, and R. C. Martineau, "Physics-based multiscale coupling for full core nuclear reactor simulation," *Annals of Nuclear Energy*, vol. 84, pp. 45–54, 2015.

[10] R. C. Martineau, "The moose multiphysics computational framework for nuclear power applications: A special issue of nuclear technology," *Nuclear Technology*, vol. 207, no. 7, pp. iii–viii, 2021.

[11] Y. Wang, S. Schunert, J. Ortensi, V. Laboure, M. DeHart, Z. Prince, F. Kong, J. Harter, P. Balestra, and F. Gleicher, "Rattlesnake: A moose-based multiphysics multischeme radiation transport application," *Nuclear Technology*, vol. 207, no. 7, pp. 1047–1072, 2021.

[12] F. N. G. J. O. et. al., "The coupling of the neutron transport application RATTLESNAKE to the fuels performance application bison," in *International Conference on Reactor Physics (PHYSOR 2014)*, (Kyoto, Japan), May 2014.

[13] Y. S. Jung and C. H. Lee, "PROTEUS-MOC User Manual," Technical Report ANL/NE-18/10, Argonne National Laboratory, September 2018.

[14] G. Marleau, A. Hébert, and R. Roy, "A user guide for dragon version5," Tech. Rep. IGE–335, Ecole Polytechnique de Montreal, 10 2020.

[15] R. Chambon, D. She, and A. Hébert, "An Improved Double Heterogeneity Model for Pebble-Bed Reactors in DRAGON-5," PHYSOR 2020, Transition to a scalable nuclear future, 2020.

[16] A. Hébert, "DRAGON5 and DONJON5, the contribution of École Polytechnique de Montréal to the SALOME platform," Third Int. Conf. on Physics and Technology of Reactors and Applications (PHYTRA3), 2014.

[17] A. Hébert, "Development of the subgroup projection method for resonance self-shielding calculations," *Nuclear Science and Engineering*, vol. 162, no. 1, pp. 56–75, 2009.

[18] Z. L. et al., "Cumulative migration method for computing rigorous diffusion coefficients and transport cross sections from Monte Carlo," *Annals of Nuclear Energy*, vol. 112, p. 507–516, 2018.

[19] A. YAMAMOTO, Y. KITAMURA, and Y. YAMANE, "Simplified treatments of anisotropic scattering in lwr core calculations," *Journal of Nuclear Science and Technology*, vol. 45, no. 3, pp. 217–229, 2008.

[20] C. Ellis and A. Baxter and D. Hanson, "Final Report – NGNP Core Performance Analysis, Phase 1," Tech. Rep. 911160, General Atomics, 2009.

[21] S. Schunert, G. Giudicelli, P. Balestra, J. Ortensi, R. Freile, and L. Harbour, "NRC multiphysics analysis capability deployment fy2021 - part 1," INL report INL/EXT-20-60777, rev. 0, Idaho National Laboratory, 12 2020.

[22] "Decay heat power in light water reactors," Tech. Rep. An American National Standard, ANSI/ANS-5.1, American Nuclear Society, 2014.

[23] A. Lindsay *et al.*, "Improvement of numerical methods in pronghorn," Tech. Rep. INL/EXT-21-65482, INL, December 2022.

[24] A. Novak, S. Schunert, R. Carlsen, P. Balestra, D. Andrs, J. Kelly, R. Slaybaugh, and M. R., "Pronghorn theory manual," Tech. Rep. INL/EXT-18-44453-Rev001, Idaho National Laboratory, 2020.

[25] S. Schunert *et al.*, "Improvements in high-temperature gas-cooled reactor modeling capabilities in the pronghorn code," Tech. Rep. INL/RPT-22-69263, INL, September 2022.

[26] S. Schunert *et al.*, "Deployment of the finite volume method in pronghorn for gas- and salt-cooled pebble-bed reactors," Tech. Rep. INL/EXT-21-63189, INL, June 2021.

[27] S. Schunert *et al.*, "Improvements in High-Temperature Gas-Cooled Reactor Modeling Capabilities in the Pronghorn Code," Tech. Rep. INL/RPT-22-69263, Idaho National Laboratory, 9 2022.

[28] R. Freile, M. Tano, P. Balestra, S. Schunert, and M. Kimber, "Improved natural convection heat transfer correlations for reactor cavity cooling systems of high-temperature gas-cooled reactors: From computational fluid dynamics to pronghorn," *Annals of Nuclear Energy*, vol. 163, p. 108547, 2021.

[29] J. Ortensi and P. Balestra, "Initial study on cross-section generation requirements for a PBR equilibrium core," PHYSOR 2021, Making Virtual a Reality - Advancements in Reactor Physics To Leap Forward Reactor Operation and Deployment, 2022.

[30] A. C. Kadak and M. Z. Bazant, "Pebble flow experiments for pebble bed reactors," 2004.